

1 **A vegetation carbon isoscape for Australia built by combining continental-**
2 **scale field surveys with remote sensing**

3

4 Samantha E.M. Munroe*^{1,2}, Greg R. Guerin^{1,2}, Francesca A. McInerney^{3,4}, Irene Martín-
5 Forés^{1,2}, Nina Welti⁵, Mark Farrell⁵, Rachel Atkins³, & Ben Sparrow^{1,2}

6

7 ¹ School of Biological Sciences, The University of Adelaide, Adelaide, South Australia 5005,
8 Australia

9 ² Terrestrial Ecosystem Research Network (TERN), University of Adelaide, Adelaide, South
10 Australia 5005, Australia

11 ³ School of Physical Sciences, The University of Adelaide, Adelaide, South Australia 5005,
12 Australia

13 ⁴ School of Earth and Environmental Sciences, University of Queensland, St. Lucia, QLD
14 4072, Australia

15 ⁵ CSIRO Agriculture and Food, Kurna Country, Urrbrae, South Australia 5064, Australia

16 *corresponding author: samantha.munroe@adelaide.edu.au

17 Author Contributions: SM originally formulated the idea, SM, as well as FM, GG, IM, NW,
18 and BS designed the study and developed the methodology. SM and GG analysed the data. MF
19 & RA contributed data and results validation; SM wrote the manuscript; all other authors
20 provided editorial advice.

21 **Acknowledgements**

22 We acknowledge the TERN Ecosystem Surveillance field team and the support of TERN by
23 the Australian government through the National Collaborative Research Infrastructure
24 Strategy. We thank Peter Scarth and David Summers for their advice on best practices for the
25 remote sensing data in our analysis.

26 **Abstract**

27 **Context:** Maps of C₃ and C₄ plant abundance and stable carbon isotope values ($\delta^{13}\text{C}$) across
28 terrestrial landscapes are valuable tools in ecology to investigate species distribution and
29 carbon exchange. Australia has a predominance of C₄-plants, thus monitoring change in
30 C₃:C₄ cover and $\delta^{13}\text{C}$ is essential to national management priorities.

31 **Objectives:** We applied a novel combination of field surveys and remote sensing data to
32 create maps of C₃ and C₄ abundance in Australia, and a vegetation $\delta^{13}\text{C}$ isoscape for the
33 continent.

34 **Methods:** We used vegetation and land-use rasters to categorize grid-cells (100 m²) into
35 woody (C₃), native herbaceous, and herbaceous cropland (C₃ and C₄) cover. Field surveys
36 and environmental factors were regressed to predict native C₄ herbaceous cover. These layers
37 were combined and a $\delta^{13}\text{C}$ mixing model was used to calculate site-averaged $\delta^{13}\text{C}$ values.

38 **Results:** Seasonal rainfall, maximum summer temperature, and soil pH were the best
39 predictors of C₄ herbaceous cover. Comparisons between predicted and observed values at
40 field sites indicated our approach reliably predicted generalised C₃:C₄ abundance. Southern
41 Australia, which has cooler temperatures and winter rainfall, was dominated by C₃ vegetation
42 and low $\delta^{13}\text{C}$ values. C₄-dominated areas included northern savannahs and grasslands.

43 **Conclusions:** Our isoscape approach is distinct because it incorporates remote sensing
44 products that calculate cover beneath the canopy, the influence of local factors, and extensive
45 validation, all of which are critical to accurate predictions. Our models can be used to predict
46 C₄:C₃ abundance under climate change, which is expected to substantially alter current C₄:C₃
47 abundance patterns.

48 **Keywords:** Photosynthesis, C₄, C₃, isoscape, carbon

49 **Declarations**

- 50 • Funding: Primary financial support for this project was provided by the Australian
51 government through the National Collaborative Research Infrastructure Strategy.
52 Additional financial support for this project was from the AMP Foundation and the AMP
53 Tomorrow Maker award presented to SM, and Australian Research Council Future
54 Fellowship (FT110100100793) awarded to FAM.
- 55 • Conflicts of interest: All authors declare they have no conflict of interest
- 56 • Ethics approval: NA
- 57 • Consent to participate: NA
- 58 • Consent for publication: All authors have provided consent to publish
- 59 • Availability of data and material: All data and relevant materials are available via open
60 access data applications, specifically via the TERN Data Discovery Portal (
61 www.portal.tern.org.au/) or the R package *ausplotsR* ([https://cran.r-](https://cran.r-project.org/web/packages/ausplotsR/index.html)
62 [project.org/web/packages/ausplotsR/index.html](https://cran.r-project.org/web/packages/ausplotsR/index.html))
- 63 • Code availability: All analysis was performed in the R environment

64

65

66 **Introduction**

67 The spatial patterns of stable carbon isotope ratios ($\delta^{13}\text{C}$) across terrestrial landscapes, also
68 known as $\delta^{13}\text{C}$ 'isoscapes', are used in a wide range of research applications (West et al.
69 2009). Most commonly, $\delta^{13}\text{C}$ isoscapes are used to study food web dynamics and animal
70 migration (Hobson et al. 2010; Hobson and Wassenaar 2018; Vander Zanden et al. 2018).
71 Animals tissues reflect the $\delta^{13}\text{C}$ value of their diet (Ben-David and Flaherty 2012; Kelly
72 2000; Tieszen et al. 1983). By comparing the carbon isotope ratios of an organism to its
73 environment, we can deduce its likely place of origin (Flockhart et al. 2017; Hobson and
74 Kardynal 2015; López-Calderón et al. 2017). Terrestrial $\delta^{13}\text{C}$ ratios can also be used to
75 unravel carbon biogeochemical fluxes (i.e. carbon exchange between the biosphere and
76 atmosphere; Still and Rastogi 2017), fractional plant productivity (Powell et al. 2012) and
77 water use efficiency (Cernusak 2020; Frank et al. 2015). Given their vast utility, creating
78 isoscapes has become a high priority in environmental research.

79
80 The primary determinant of average vegetation $\delta^{13}\text{C}$ values across terrestrial landscapes is the
81 relative abundance of C_3 and C_4 plants (Still et al. 2003). C_3 plants include cool season
82 grasses, most shrubs, and nearly all trees (Kellogg 2001; Sage 2016), whereas C_4 plants
83 include warm-season grasses, many sedges, and some forbs and shrubs (Sage et al. 2012).
84 The distribution of C_3 and C_4 plants reflects their divergent responses to climate. In hot and
85 dry environments, C_3 plants experience increased rates of oxygen fixation by rubisco
86 (photorespiration), a toxic and energetically expensive process, and diminishing returns in the
87 trade-off between carbon uptake and water loss (Andrews and Lorimer 1987; Sage et al.
88 2012). In contrast, C_4 plants possess a unique set of adaptations that separate and concentrate
89 CO_2 with rubisco, eliminating photorespiration and increasing productivity in hot and dry

90 conditions (Kanai and Edwards 1999; Sage 2004). As a result, C₃ plants are typically less
91 competitive in warm, arid climates. C₃ and C₄ plants also have a unique range of $\delta^{13}\text{C}$ values.
92 Due to their distinct carbon fractionation processes during photosynthesis, the values of C₃
93 plants range from -37‰ to -20‰ $\delta^{13}\text{C}$ (mean= ~-27‰), and the values of C₄ plants range
94 from -12‰ to -16‰ $\delta^{13}\text{C}$ (mean=~-13‰; Kohn 2010; O'Leary 1988). Therefore, knowledge
95 of C₃ and C₄ cover can be used to estimate average plant $\delta^{13}\text{C}$ across terrestrial environments
96 (Powell et al. 2012; Still and Powell 2010).

97

98 Remote sensing capabilities can be used to approximate C₃ and C₄ cover at a continental
99 scale (Griffith et al. 2019; Powell et al. 2012; Still and Powell 2010). Satellite imagery
100 enables the separation of woody (predominantly C₃) and herbaceous (mixed C₃ and C₄) plant
101 cover. Climate masks or models can be used to predict the relative abundance of C₄ and C₃
102 cover in the herbaceous layer, and the $\delta^{13}\text{C}$ values of C₃ and C₄ plants can be applied to
103 extrapolate the mean $\delta^{13}\text{C}$ value of vegetation in a given area. Cropland cover must also be
104 considered because the photosynthetic pathway of cropland is dictated by humans, not
105 climate. This technique has been applied to create terrestrial $\delta^{13}\text{C}$ isoscapes at the continental
106 scale in Africa and America (Firmin 2016; Powell et al. 2012; Still and Powell 2010),
107 although other continents undergoing profound land-use changes remain unassessed.

108

109 Field surveys can greatly enhance the accuracy of $\delta^{13}\text{C}$ isoscapes. Vegetation cover data from
110 field surveys can be used to compare different C₄ cover-climate models and determine what
111 approach should be used to predict the relative abundance of C₄ and C₃ herbaceous cover.
112 Numerous models have been proposed to predict relative C₄ herbaceous cover, such as
113 summer maximum temperatures (von Fischer et al. 2008) and seasonal rainfall patterns

114 (Murphy and Bowman 2007; Winslow et al. 2003). The most commonly employed approach
115 is the physiological temperature crossover model (Collatz et al. 1998; Ehleringer 1978),
116 which predicts C₄ plants will be more abundant in areas where the mean monthly temperature
117 is greater than 22°C. The best approach may vary between regions, therefore selecting the
118 most appropriate model for a specific area is essential for accurate isoscape predictions. Field
119 surveys can also be used to model the modifying effects of local edaphic factors on C₄ cover
120 (Griffith et al. 2015; Nippert and Knapp 2007), which is generally overlooked in large-scale
121 analysis. They can be used to quantify the herbaceous cover under trees, which is often
122 obscured, and thus excluded, from isoscapes built using standard remote sensing tools.
123 Finally, but perhaps most crucially, field surveys can validate remote sensing predictions.
124 Yet, systematic and comparable field surveys that span an entire continent are rare, and
125 existing large-scale isoscapes have been largely constructed without the benefits of ground
126 observations or extensive validation.

127
128 Australia is a continent with abundant C₄ vegetation due to the large expanses of C₄
129 grasslands, shrublands and savannahs (Hattersley 1983; Murphy and Bowman 2007; Sage
130 2016). Therefore, monitoring and predicting trends in C₄ abundance and $\delta^{13}\text{C}$ is important to
131 national management priorities, such as fire modelling (Prober et al. 2007) and projecting
132 changes in C₃ and C₄ abundance due to climate change (Corlett and Westcott 2013;
133 Hasegawa et al. 2018). Despite this, no large-scale estimates of C₃ or C₄ vegetation cover or
134 $\delta^{13}\text{C}$ values are available. This represents a significant gap in national research capacity. The
135 Australian Terrestrial Ecosystem Research Network (TERN) is an environmental monitoring
136 program funded through the Australian Government National Collaborative Research
137 Infrastructure Strategy (NCRIS) that observes, records, and measures terrestrial ecosystem
138 parameters and conditions for Australia over time. TERN has developed numerous remote

139 sensing layers that estimate the relative distribution of vegetation cover across the country
140 (see www.tern.org). TERN has also conducted over 700, one ha plot-based vegetation
141 surveys across all major biomes and dryland habitats. These combined resources provide a
142 novel opportunity to advance and validate remote sensing strategies for building large
143 terrestrial isoscapes, and for the first time develop a $\delta^{13}\text{C}$ isoscape for Australia.

144

145 The goals of this paper were to create mapping products that represent the distribution of C_3
146 and C_4 vegetation in Australia, and construct a site-averaged vegetation $\delta^{13}\text{C}$ isoscape for the
147 continent (including Tasmania) using a unique combination of field surveys and remote
148 sensing tools. To create a terrestrial vegetation $\delta^{13}\text{C}$ isoscape, we adapted the methodology
149 pioneered by Still and Powell (2010) and Powell et al. (2012), with key modifications that
150 benefit from Australian ground survey data and advancements in remote sensing. To predict
151 the relative cover of C_3 and C_4 vegetation, we used vegetation and climate rasters to (1)
152 categorize grid-cells (100 m^2) into woody (C_3) and herbaceous (C_3 and C_4) components, (2)
153 determine the extent of Australian cropland and assign each crop a photosynthetic type (i.e.
154 C_3 or C_4), and (3) apply a % herbaceous C_4 cover~climate and edaphic model to predict
155 proportional (%) C_3 and C_4 herbaceous cover. In contrast to other large-scale isoscapes,
156 TERN remote sensing data and field surveys were used to account for the ground cover
157 fraction beneath the vegetation canopy, and the influence of local-scale factors on C_4
158 abundance. Once relative C_3 and C_4 vegetation cover layers were generated, we used a $\delta^{13}\text{C}$
159 mixing model to determine the average vegetation $\delta^{13}\text{C}$ value in each grid-cell. We also
160 conducted novel accuracy assessments of our final predictions across major vegetation
161 groups and demonstrate the research potential of these data layers with an example of C_4 -
162 landscape analysis across all bioregions in Australia. Our results provide an alternative
163 approach to constructing terrestrial $\delta^{13}\text{C}$ isoscapes that may better incorporate local-scale

164 controls on C₃:C₄ abundance and enables the prediction of future changes in C₃ and C₄
165 distribution under various climate change scenarios. This is a critical feature of our
166 methodology, as climate change is anticipated to drastically shift the competitive advantage
167 of C₃ and C₄ plants across the continent.

168

169 **Methods**

170 **Step 1: Estimate % woody and % herbaceous cover**

171 Our Australian $\delta^{13}\text{C}$ vegetation isoscape was constructed using remote sensing vegetation
172 data primarily sourced for the year 2015. Climate conditions in 2015 for Australia were
173 considered average (i.e. not dry or wet), and fire occurrence and intensity were relatively low.
174 This was also one of the most recent years for which exhaustive vegetation data were
175 available. Thus, a 2015 isoscape should be a good representation of modern average
176 conditions in Australia.

177

178 To create the isoscape, we adapted the methodology of Still and Powell (2010) and Powell et
179 al. (2012) and partitioned Australian vegetation cover into C₃ and C₄ cover layers (Fig. 1).
180 The % *woody cover* layer was generated from the Seasonal Persistent Green Cover product
181 for Australia (Gill et al. 2017; Gill et al. 2015). This product is derived from Landsat 5 TM,
182 Landsat 7 ETM+ and Landsat 8 OLI images acquired from the United States Geological
183 Survey (USGS) and estimates the proportion (%) of green fractional cover (i.e. the fraction of
184 ground covered by green vegetation) that does not entirely deteriorate within a year (see
185 Supplemental Methods Table 1 for synopsis of all datasets). This primarily consists of woody
186 vegetation (i.e. trees and shrubs). Estimates for Seasonal Persistent Green Cover and
187 projected woody foliage cover (2000-2010) have been validated with field-measurements,

188 providing an R^2 of 0.918 and a root mean square error (RMSE) of 0.070. The overall
189 classification accuracy of the woody vegetation extent is 81.9%. Based on these results, we
190 treated % *woody cover* as the most accurate estimate for any cover product in our analysis.

191

192 The % *herbaceous cover* layer was generated from the Seasonal Fractional Ground Cover
193 product for Australia (Trevithick et al. 2014). The Seasonal Fractional Ground Cover product
194 is derived from the Seasonal Fractional Cover time series and the Seasonal Persistent Green
195 Cover product. It consists of three components, (1) % vegetated green (photosynthetically
196 active) ground cover, (2) % vegetated non-green (i.e. non-photosynthetic) ground cover
197 (primarily dead vegetation), and (3) % bare ground. These three components sum to 100%.

198 The Seasonal Fractional Ground Cover is distinct from other remote sensing measures of
199 fractional ground cover because it accounts for vegetation layering. The Seasonal Fractional
200 Ground Cover includes the ground cover fraction that is visible to the satellite (i.e. viewed
201 from above), but also applies a model to account for the ground cover fraction that may grow
202 beneath the vegetation canopy. Essentially, the Seasonal Fractional Ground Cover predicts
203 the ground cover under the canopy that is normally obscured from the view of the satellite.

204 This provides a potentially more accurate representation of ‘true’ ground cover compared to
205 other remote sensing data. Vegetated green and vegetated non-green ground cover were
206 combined to estimate the total % *herbaceous cover* in each grid-cell. Vegetated non-green
207 ground cover was included in % *herbaceous cover* to account for Australia’s highly arid

208 climate and ensure that wide spread senescent vegetation was incorporated into our
209 calculations. Both % *woody* and % *herbaceous cover* predicts vegetation cover at medium
210 resolution (30 m) for each calendar season (3 months) and are freely available from the

211 TERN Landscape Monitoring’s Remote Sensing Data Facility. To bring cover data to a scale
212 consistent with the other data products, we resampled all vegetation raster layers to a

213 resolution of 100 m x 100 m per pixel (1 ha). Values from each season were combined to
214 calculate the annual mean % *woody* and % *herbaceous cover* (Fig. 2).

215 Estimates of Seasonal Fractional Ground Cover were restricted to areas of < 60 % *woody*
216 *cover* because the model used to estimate the herbaceous cover under trees is not effective in
217 dense forests. TERN plot data indicated in areas where tree cover was > 60%, herbaceous
218 cover was limited and ranged from 0 to 25% (Supplemental Methods Figure 1). This is
219 consistent with other work demonstrating increased canopy cover can reduce herbaceous
220 cover due to reduced light availability in the understory (Cole and Weltzin 2005; Dormann et
221 al. 2020). Therefore, in grid cells with > 60% *woody cover*, % *herbaceous cover* was
222 presumed to be minimal and set to zero (see Supplemental Methods for full justification).

223

224 The % *woody cover* layer was designated 100% C₃ vegetation. This introduces a potential
225 source of error because some groups of shrubs, in particular chenopods, may use either C₃ or
226 C₄ photosynthesis (Akhani et al. 1997; Munroe et al. 2020b). However, chenopods are mostly
227 evergreen and are likely largely incorporated into the % *woody cover* fraction (Scarth,
228 personal communication). We were unable to identify an accurate way to distinguish and
229 model C₄ chenopod shrub cover from other woody cover across Australia. Remote sensing
230 does not relate well to chenopod vegetation (O'Neill 1996; Sparrow et al. 1997), and
231 statistical analysis of TERN field plot found proportional C₄ chenopod distribution (relative
232 to C₃) is not closely associated with climate in Australia (Munroe et al. in review).
233 Consequently, we made the simplifying assumption that all woody cover is C₃.

234

235 **Step 2: Incorporate agro-ecosystems**

236 The photosynthetic pathway of cropland is determined by what type of crop is planted in each
237 area. Therefore, the photosynthetic pathway of crops must be evaluated separately to natural
238 vegetation. To accomplish this, we partitioned % *herbaceous cover* into % *natural*
239 *herbaceous cover* and % *herbaceous crop cover* layers. This was achieved using the
240 Catchment Scale Land Use of Australia (CLUM) dataset. The CLUM dataset is the most
241 current, nationally consistent compilation of catchment scale land use data for Australia
242 (current as of December 2018). It is a seamless raster dataset that combines land use data for
243 all state and territory jurisdictions at a resolution of 50 metres. The CLUM dataset indicates a
244 single dominant land use type for each grid-cell. Land use is classified according to
245 the Australian Land Use and Management (ALUM) Classification version 8 (ABARES
246 2016). This dataset identifies cropping land across the country, and includes information on
247 specific commodities (e.g. sugar, rice, cereals). Using CLUM, we determined the
248 geographical extent of herbaceous cropland areas. We assumed that in cropland grid-cells,
249 100% of the % *herbaceous cover* was crops. Based on this assumption, % *herbaceous cover*
250 was divided into % *natural herbaceous cover* and % *herbaceous crop cover* layers (Fig 3).
251 Using the CLUM dataset, we then determined the likely commodity and photosynthetic type
252 planted at each grid-cell in the % *herbaceous crop cover* layer.

253

254 Most identified crops in Australia were C₃ (e.g. wheat, barley, rice). The only specifically
255 identified C₄ commodity was sugarcane. However, the generic ALUM classifications ‘cereal
256 crops’ and ‘crops’, which were the most common and extensive crop designations in the
257 CLUM dataset, may be C₃ or C₄ grain. To assess the likelihood of ‘cereal crops’ and ‘crops’
258 being C₃ or C₄, we consulted the Australian Bureau of Statistics (ABS), which conducts
259 detailed agricultural censuses that quantify crop area, commodity type, production, and yield
260 data for Australia, each state/territory, and sub-state regions. The most recent relevant

261 agriculture census was for 2015/16 (ABS 2016). According to ABS (2016), the most
262 common C₄ grain crops in Australia are sorghum and maize. Together, sorghum and maize
263 only equalled approximately 2% of the total cropping area (ha) in Australia in 2015. Most
264 sorghum and maize were grown in the so-called ‘sorghum belt’, which stretches across the
265 southern cropping regions of Queensland and the northern cropping areas of New South
266 Wales. Within this area, sorghum and maize represent less than 15% of the cropping area. In
267 addition, sorghum is often seasonally rotated with wheat. Without more specific information
268 on the cropping locations for sorghum and maize, and given its likely limited land cover in
269 2015, we determined that unspecified cropland should be assigned 100% C₃. Using these
270 finalised C₃ and C₄ cropland assignments, % *herbaceous crop cover* was subdivided into %
271 *herbaceous C₃ crop cover* and % *herbaceous C₄ crop cover* layers.

272

273 **Step 3: Assign % natural herbaceous cover layer proportional C₃ and C₄ values**

274 % *natural herbaceous cover* includes a mix of C₃ and C₄ plants whose relative abundance is
275 dictated by climate and local environmental conditions. Therefore, to estimate the relative
276 cover of C₃ and C₄ plants in each grid-cell of the % *natural herbaceous cover* layer, we
277 applied a statistical model that accounts for their divergent responses to climate and edaphic
278 factors. We used TERN vegetation survey data to compare various environmental models to
279 identify the most accurate method for predicting proportional (%) herbaceous C₄ vegetation
280 across Australia.

281

282 *Step 3a. Create a model to predict proportional (%) herbaceous C₄ vegetation cover*

283 We calculated proportional (%) herbaceous C₄ vegetation cover (relative to herbaceous C₃
284 and C₄ cover) at 700 one-hectare plots systemically surveyed using a point-intercept method
285 by TERN between 2011 and 2019. A full description of TERN plot survey protocols is

286 detailed in the TERN AusPlots Rangeland manual (Sparrow et al. 2020; White et al. 2012).
287 The protocols most relevant to our analysis are documented in the Supplemental methods.
288 TERN plot data were analysed in the R statistical environment (R Core Team 2019) and
289 imported using the ‘ausplotsR’ package (Guerin et al. 2020; Munroe et al. 2020a), a package
290 which enables the import and analysis TERN plot survey data. Herbaceous species cover (%)
291 was calculated at each TERN plot using the *species_table* function. Species were assigned a
292 photosynthetic pathway using Munroe et al. (2020b). Herbaceous species included the growth
293 forms 'Forb', 'Hummock grass', 'Rush', 'Sedge', and 'Tussock grass'. Proportional herbaceous
294 C₄ cover at TERN plots (Fig 4) was then calculated as a proportion of C₃ and C₄ herbaceous
295 species cover by:

296 **Eq 1** Proportional herbaceous C₄ cover = C₄ herbaceous species cover/
297 (C₄ herbaceous species cover + C₃ herbaceous species cover)

300 We then compiled a dataset of climatic and edaphic variables (Supplemental Methods Table
301 3) that are considered potential drivers of C₄ plant distribution (Griffith et al. 2015; Pau et al.
302 2013; Sage 2004). Climate data layers were sourced from Williams et al. (2010) and edaphic
303 data from Gallant et al. (2018). We also considered the Collatz et al. (1998) crossover
304 temperature model for comparison (Collatz et al. 1998; Ehleringer 1978). Using this
305 approach, a particular month is determined to favour C₄ growth when the mean daytime
306 temperature was > 22 °C and precipitation is ≥ 25 mm, while a particular month is
307 determined to favour C₃ growth when the mean daytime temperature was ≤ 22 °C and
308 precipitation is ≥ 25 mm. However, because large areas of Australia receive < 25 mm of
309 precipitation per month, a traditional crossover approach may not be accurate (Murphy and
310 Bowman 2007). Therefore, to apply the crossover temperature model consistently across the
311 country, we regressed proportional C₄ herbaceous cover against the mean annual proportion

312 of C₄ favoured months (> 22 °C and ≥ 25 mm rainfall), instead of the absolute number of C₄
313 favoured months (Munroe et al. in review). Climate data for the crossover approach were
314 calculated using 1970–2018 records from the Australian Gridded Climate Data set (Bureau of
315 Meteorology). Australian Gridded Climate Data were required to calculate monthly values
316 for the crossover temperature model because unlike Williams et al. (2010), it provides daily
317 data.

318

319 To relate proportional herbaceous C₄ cover at each plot to climate and soil data, we used a
320 generalised additive model (GAM) approach. GAMs were chosen because they can
321 accommodate non-linear effects (Wood 2006; Wood 2017) and can be specified to account
322 for high spatial autocorrelation (see discussion below; Zuur et al. 2009). Because C₄ plot
323 cover data was proportional with ‘true’ values of 0 and 1, we used a logistic error structure
324 (Douma and Weedon 2019). The smooth functions of each variable were limited to five
325 degrees of freedom. This allowed for nonlinearity in the data while avoiding overfitting.
326 Models were limited to variables that had Pearson pairwise correlations < 0.8 and interaction
327 terms were not included. Models were compared using a step-wise, forward-selection
328 procedure and Akaike information criterion (AIC). Model fit was measured using R². Models
329 were constructed using the *gamm* function in the *mgcv* package (Wood 2021).

330

331 Moran's I tests confirmed the presence of spatial autocorrelation in preliminary GAM
332 residuals (Matthews et al. 2019). Spatial autocorrelation can reduce model precision and
333 predictive power (Guélat and Kéry 2018; Mets et al. 2017). Spatial autocorrelation can be
334 alleviated by either (a) including spatial coordinates (i.e. longitude, latitude) in the model as
335 covariates, or by (b) accounting for spatial autocorrelation in model residuals. The former can

336 be problematic because spatial coordinates typically co-vary with environmental variables.
337 Therefore, we incorporated a correlation structure in the model residuals.

338

339 *Step3b. Extrapolate proportional herbaceous C₄ and C₃ cover*

340 Model AIC comparisons indicated the best model to predict proportional herbaceous C₄ cover
341 included the ratio (log) of summer (Dec-Jan-Feb) to winter (Jun-Jul-Aug) rainfall (slrain1),
342 the maximum temperature of the hottest month (maxtx), and soil pH-CaCl₂ (PHC), sand
343 content (%; SND), and available water capacity (%; AWC) as variables (R²=0.7;
344 Supplemental Results Table 4). As maxtx, slrain1 and PHC increased (i.e. pH becomes more
345 alkaline), proportional herbaceous C₄ cover generally increased (Fig 5 a,b,c). The effects of
346 sand content and AWC were nonlinear (Fig 5 e,f), where proportional herbaceous C₄ cover
347 was predicted to be higher in plots where both soil sand content and AWC exhibited more
348 extreme values. However, these nonlinear trends may have been driven by the relative
349 paucity of data in areas with low sand content (<40%) and AWC (<12%). The resulting
350 GAM was extrapolated across the Australian continent (Fig 6) and used to predict
351 proportional herbaceous C₄ cover in each grid-cell of the *% natural herbaceous cover* layer
352 and generate a *% natural herbaceous C₄ cover* layer. A *% natural herbaceous C₃ cover* layer
353 was calculated by subtracting the *% natural herbaceous C₄ cover* layer from the original *%*
354 *natural herbaceous cover* layer.

355

356 **Step 4: Create final C₃ and C₄ vegetation layers**

357 To finalise the C₃ and C₄ cover vegetation layers, all C₃ vegetation layers were summed to
358 create a single *% C₃ cover* layer (Fig 7a).

359

360 **Eq 2** $\% C_3 \text{ crop cover} + \% \text{ natural herbaceous } C_3 \text{ cover} + \% \text{ woody vegetation} = \% C_3 \text{ cover}$

361

362 Similarly, C_4 vegetation layers were summed to create a single $\% C_4 \text{ cover}$ layer (Fig 7b).

363 **Eq 3** $\% C_4 \text{ crop cover} + \% \text{ natural herbaceous } C_4 \text{ cover} = \% C_4 \text{ cover}$

364

365 Finally, both $\% C_3$ and $C_4 \text{ cover}$ layers were converted from $\% \text{ cover}$ to $\% \text{ vegetation}$. This is

366 because many areas will have a high percentage of bare ground that is irrelevant to

367 calculating the final isoscape. The $\% \text{ vegetation}$ was calculated as:

368 .

369 **Eq 4** $\% \text{ vegetation} = \% \text{ cover of vegetation type} / \% \text{ total vegetation cover}$.

370

371 This resulted in the final two layers, $\% C_3 \text{ vegetation}$ and $\% C_4 \text{ vegetation}$ (Fig 7c,d)

372

373 **Step 5: Calculate site-averaged vegetation $\delta^{13}\text{C}$ using a two end-member mixing model**

374 The average vegetation $\delta^{13}\text{C}$ value for each grid-cell was calculated based on the final $\% C_3$

375 vegetation and $\% C_4 \text{ vegetation}$ layers and a $\delta^{13}\text{C}$ mixing model. End-members were derived

376 from the literature. Previous work has indicated that understory plants in closed canopy

377 environments have lower $\delta^{13}\text{C}$ values than open forests (Cheesman et al. 2020; Powell et al.

378 2012); however, the bulk of leaf mass resides in the upper canopy. Moreover, this effect is

379 typically most exaggerated in dense rainforest habitats, which represent a minute porportion of

380 the total land area in Australia. Therefore, we opted not to apply a canopy cover correction to

381 average vegetation $\delta^{13}\text{C}$ values because (a) there was enough data to calculate a reliable

382 correction value, and (b) such a correction was not deemed useful at this resolution. Previous

383 work has also applied different end-member $\delta^{13}\text{C}$ values for herbaceous and woody C_3

384 vegetation (Firmin 2016). However work by Pate et al. (1998) and data from Munroe et al.

385 (2020b) did not identify significant differences in $\delta^{13}\text{C}$ between C_3 herbaceous and C_3
386 woody species. Thus, for simplicity, using values from Munroe et al. (2020b), we calculated
387 the mean \pm sd $\delta^{13}\text{C}$ values for C_4 and C_3 (herbaceous and woody) endmembers. The mean \pm sd
388 of $\delta^{13}\text{C}$ values for C_4 herbaceous plants was $-13.8 \pm 1.1\text{‰}$ (n=119), and for C_3
389 herbaceous/woody plants was $-27.7 \pm 2.3\text{‰}$ (n=420).

390

391 The site-averaged vegetation $\delta^{13}\text{C}$ isoscape was then calculated using a Monte Carlo method
392 and a simple mixing model:

393

394 **Eq 5** $\delta^{13}\text{C}_{\text{leaf}} = f_{\text{C}_4\text{veg}} * (\delta^{13}\text{C}_{\text{C}_4\text{veg}}) + f_{\text{C}_3\text{veg}} * (\delta^{13}\text{C}_{\text{C}_3\text{veg}})$

395

396 $f_{\text{C}_4\text{veg}} = \% \text{C}_4 \text{ vegetation}$

397

398 $f_{\text{C}_3\text{veg}} = \% \text{C}_3 \text{ vegetation}$

399 Different possible values of $\delta^{13}\text{C}_{\text{C}_4\text{veg}}$ and $\delta^{13}\text{C}_{\text{C}_3\text{veg}}$ from the range of possible $\delta^{13}\text{C}$ values
400 (mean $\pm 2 * \text{sd}$) determined from Munroe et al. (2020b) were randomly substituted into Eq 5
401 for 1000 iterations. The results were averaged to produce the final vegetation $\delta^{13}\text{C}$ isoscape.
402 A standard deviation raster was created by calculating the standard deviation of the 1000
403 iterations of each grid cell (Fig. 8).

404

405 **Step 6. Validation**

406 To validate model outcomes and the final vegetation $\delta^{13}\text{C}$ isoscape, we calculated the root
407 mean squared error (RMSE) of competing % herbaceous C_4 cover ~ climate models (Bataille
408 et al. 2018). The RMSE of each model was calculated using 10-fold cross-validation where
409 the original dataset was randomly split ten times between a training data set (90% of plots)
410 and a testing dataset (10% of plots). To assess the accuracy of the final % C_4 vegetation layer,
411 we compared the predicted % C_4 vegetation layer outputs to the proportional % C_4 vegetation

412 cover observed at all TERN plots. We used a linear regression to quantify relationships
413 between predicted and observed % *C₄ vegetation* values. We also compared the residual
414 values of predicted and observed % *C₄ vegetation* in different major vegetation groups
415 (MVG), as determined by onsite evaluations by TERN survey teams.

416

417 Finally, we compared predicted leaf- $\delta^{13}\text{C}$ values to soil organic matter (SOM) $\delta^{13}\text{C}$ values
418 determined samples collected at TERN plots. SOM $\delta^{13}\text{C}$ values were provided from two
419 separate projects. Soil samples were collected at 19 TERN plots between 2011 and 2013 and
420 analysed in 2019 as part of a project testing different isotopic tools to predict % *C₄* abundance
421 (Atkins 2020). These plots are located along a North to South transect through central
422 Australia (Supplemental Methods Figure 4). For this project, a single soil sample was
423 collected from the top 3 cm of the soil profile at the same location in each plot. Additional
424 SOM $\delta^{13}\text{C}$ values were provided from 32 TERN plots located along the Adelaide
425 Geosyncline in South Australia as part of a project examining the relationship between soil
426 isotopic composition and aridity (Farrell, unpublished data). In April and May 2016, 20 soil
427 samples were taken at random within each plot from the 0-10 cm layer; the 20 samples were
428 composited and homogenised in the field to yield a single representative 0-10 cm soil sample
429 for each plot. Atkins (2020) 0-3 cm depth SOM $\delta^{13}\text{C}$ values were adjusted by 0.5‰ and
430 Farrell 0-10 cm depth SOM $\delta^{13}\text{C}$ values by 1‰ to account for ^{13}C enrichment during
431 decomposition in SOM (Krull and Bray 2005). Like % *C₄ vegetation* comparisons, we
432 calculated the residuals for SOM-adjusted and predicted leaf $\delta^{13}\text{C}$ values and used a linear
433 regression to compare predicted and measured results.

434

435 **Applications**

436 To demonstrate the analytical potential for landscape research with these vegetation data
437 layers, we used the % C_4 and C_3 *vegetation cover* layers and leaf- $\delta^{13}C$ isoscape to calculate
438 the mean C_4 and C_3 cover and leaf- $\delta^{13}C$ values of 86 different continental Australian
439 bioregions, as described by the interim Biogeographic Regionalisation for Australia version 7
440 (IBRA 7.0; Department of Agriculture, Water and the Environment, 2020). Bioregions are
441 large, geographically distinct areas that share common characteristics such as climate,
442 landform patterns, and plant and animal communities. These regions are used to help identify
443 unique ecosystems within Australia. Thus, understanding differences in C_3 and C_4 cover
444 between these regions is critical to identifying their unique attributes and vulnerabilities. Here
445 we compared mean proportional C_3 and C_4 cover and leaf- $\delta^{13}C$ in each bioregion to trends
446 *slrain1* and % *woody* and *herbaceous cover*.

447

448 **Results**

449 **Geographic distribution of vegetation $\delta^{13}C$ in Australia**

450 Our stepwise procedures produced 9 data layers representing C_4 and C_3 distribution in both
451 agricultural and native environments. Predicted % C_3 and C_4 *vegetation* maps and the $\delta^{13}C$
452 leaf isoscape followed expected trends in C_3 and C_4 vegetation (Fig 7 and 8). Southern areas
453 of the country, which are characterised by cooler temperatures and high winter rainfall, were
454 dominated by large areas of C_3 cropland and woody vegetation, and thus had the most
455 negative $\delta^{13}C$ values. Mid-western and eastern coastal regions also have a large proportion of
456 C_3 vegetation, including a mix of forests, cropland, and herbaceous vegetation, and have
457 correspondingly low $\delta^{13}C$ values. C_4 -dominated and isotopically ^{13}C -enriched areas
458 predominately included northern savannahs and grasslands.

459

460 The south to north transition from C₃ to C₄ dominated areas, and more negative to less
461 negative $\delta^{13}\text{C}$ values, was abrupt. The clear demarcation between C₃ and C₄ habitats is
462 consistent with the relatively rapid transition from winter to summer dominated rainfall
463 patterns across the country. Central areas of Australia are arid and receive sporadic rainfall
464 with high inter-annual variability. As a result, there is relatively low and sparse woody cover
465 and conditions do not support most C₃ herbaceous plants. The apparent exception to this is
466 the Simpson Desert, located in central Australia across South Australia and the Northern
467 Territory. Although C₃ cover in the Simpson Desert was low and consistent with surrounding
468 areas, this region has notably lower C₄ herbaceous cover compared to other nearby
469 environments, leading to lower proportional C₄ vegetation cover and $\delta^{13}\text{C}$ values. This due to
470 the extremely dry conditions (< 50 mm rainfall/year) in the desert which make it difficult for
471 any herbaceous plants to grow.

472

473 **Validation**

474 As previously described, the best model to predict proportional herbaceous C₄ cover included
475 slrain1, maxtx, PHC, SND, and AWC as variables. The proportional herbaceous C₄-climate
476 GAM used to predict C₄ cover had a mean RMSE of 27.8% \pm 2.0. Linear regression analysis
477 comparing predicted and observed proportional herbaceous C₄ vegetation cover resulted in an
478 adjusted-R² of 0.54 (Fig 9a). Comparisons between predicted and observed % C₄ vegetation
479 (including woody cover) at TERN plots returned residuals ranging from -63.4 to 73.4%
480 (mean \pm sd = 9.1 \pm 24.5) and a RMSE of 26.1%. This suggests that, on average, our approach
481 overestimates relative C₄ cover. Linear regression analysis comparing predicted and observed
482 proportional C₄ vegetation cover resulted in an adjusted-R² of 0.44 (Fig 9b).

483

484 Most TERN plots were located in Eucalypt woodlands, followed by Tussock grasslands,
485 Chenopod shrublands, and Acacia woodlands. Comparisons of residuals between major
486 vegetation group classifications revealed that residuals were smallest in heathlands, Eucalypt
487 woodlands and forests, and tussock grasses, but were largest in Acacia- and Melaleuca-
488 dominated habitats (Supplemental Results Table 2; Fig 10). The spread in the residuals for
489 each MVG indicated that C₄ cover was generally overestimated in most habitats but was
490 underestimated in grasslands.

491

492 Comparisons between predicted leaf and soil $\delta^{13}\text{C}$ isotope values returned a RMSE of 2.1‰.
493 Residuals ranged from -5.40‰ to 5.44‰ with a mean value of 0.26‰ (± 2.12). The line of
494 best fit between these variables had a slope of 0.74, an intercept of -6.0, and an adjusted-R² of
495 0.71 (Fig 9c). These results indicate that on average the isoscape overestimated mean leaf
496 $\delta^{13}\text{C}$ values (i.e. were less negative), which is consistent with comparisons between predicted
497 and observed % C₄ vegetation.

498

499 **IBRA Analysis**

500 Bioregions with the greatest proportional C₃ cover were located Tasmania, southern
501 Australia, and the Australian Alps (100% C₃ cover; Supplemental Results, IBRA Analysis).
502 Bioregions with the greatest C₄ cover included the Central Kimberly, Mitchell Grass Downs,
503 and Gulf Plains (> 75% C₄ cover). Across all bioregions, we found an increasing trend of
504 proportional C₃ cover with increased % woody cover (Fig. 11a), but no relationship between
505 increased herbaceous cover and proportional C₄ cover (Fig. 11b). There was also a clear non-
506 linear relationship between slrain1 and mean proportional C₃ cover; where slrain1 increased,
507 there was a rapid decline in % C₃ cover (Fig. 11c). This is mirrored by an increase in mean
508 predicted leaf- $\delta^{13}\text{C}$ with increased slrain1.

509 **Discussion**

510 We leveraged a novel combination of field surveys and remote sensing data to create national
511 C₃ and C₄ vegetation maps and a $\delta^{13}\text{C}$ vegetation isoscape for Australia. The good agreement
512 between our predictions and observed values indicates our approach can provide valuable
513 generalized depictions of C₄ and $\delta^{13}\text{C}$ -leaf variation across diverse landscapes at large scales.
514 Our approach benefits from recent advancements in remote sensing by being the first to
515 incorporate vegetation layering, which is critical to accurate representations of C₃:C₄ trends.
516 Our work also demonstrates the value of extensive field surveys when constructing and
517 validating isoscape projections in different regions, by providing the unique ability to
518 incorporate edaphic variables into large-scale models. This is particularly impressive
519 considering the ground survey vegetation data used to construct the final outputs were
520 collected by TERN over a period of 9 years, both before and after the 2015 remote sensing
521 time-slice used to create the isoscape. Most of these plots have only been surveyed once and
522 thus describe a snap-shot in time from a single season. Therefore, an average error rate of
523 ~25% represents a significant level of overall accuracy. Comparisons between predicted leaf-
524 $\delta^{13}\text{C}$ values to measured $\delta^{13}\text{C}$ soil values achieved a stronger correlation than comparisons to
525 ground surveys. The stronger correlation may be because soil $\delta^{13}\text{C}$ represents long-term
526 averages in relative C₄ vegetation cover. Our $\delta^{13}\text{C}$ validation results are consistent with the
527 level of accuracy achieved by other $\delta^{13}\text{C}$ isoscapes developed using remote sensing
528 techniques in North and South America (Powell et al. 2012, Firmin 2016). Overall, the
529 relatively high level of accuracy in our C₄ and $\delta^{13}\text{C}$ predictions demonstrates remote sensing
530 combined with field surveys can provide useful, generalized C₄ maps and $\delta^{13}\text{C}$ isoscapes, and
531 informative estimations on C₃:C₄ vegetation cover over diverse landscapes in areas where
532 data is limited.

533

534 **Modelling herbaceous C₄ and C₃ distribution**

535 The best model for predicting proportional C₄ herbaceous cover included maximum summer
536 temperature and seasonal rainfall ratios as climate variables. This is consistent with previous
537 work indicating both C₄ grass and sedge cover is predominantly correlated with January
538 temperatures and proportional summer rainfall (Murphy and Bowman 2007; von Fischer et
539 al. 2008). Interestingly, the crossover temperature model was one of the least accurate climate
540 models and was difficult to apply consistently across Australia. These findings are consistent
541 with Munroe et al (2022) and Xie et al (2022), who also found that seasonal rainfall ratios
542 and summer temperatures were better predictors of C₄ grass abundance than the crossover
543 temperature model. Although we acknowledge that the crossover approach was never
544 intended to delineate fine-scale distribution patterns, our results demonstrate this approach is
545 not the best method to determine C₄ distribution in Australia.

546
547 Local edaphic factors were also selected in the best fit model. Previous work has
548 demonstrated local environmental factors can significantly modify herbaceous C₄ distribution
549 (Griffith et al. 2015; Nippert and Knapp 2007; Wang et al. 2020). Our work suggests pH has
550 a significant positive influence on relative C₄ herbaceous cover and should be considered
551 even in continental models. The influence of alkaline-stress on C₄ versus C₃ plants is not well
552 understood, but C₄ plants are thought to be more resistant to stress and therefore more
553 tolerant to alkaline soil (Bromham et al. 2013; Sage 2004; Saslis-Lagoudakis et al. 2014).
554 However, pH is often related or correlated with other climate and soil conditions like salinity
555 and rainfall, thus the observed effect of pH may reflect underlying factors not included in our
556 analysis (James et al. 2005; Saslis-Lagoudakis et al. 2014). Isolating the impacts of available
557 water capacity and sand content is more difficult given its apparent nonlinear relationship to
558 C₄ cover, but together they may indicate a significant impact of changes in local moisture

559 availability, which can affect competitive dynamics between C₃ and C₄ species (Nippert and
560 Knapp 2007; Sage 2004).

561

562 **Limitations and Uncertainty**

563 The proportional herbaceous C₄ cover model tended to underestimate C₄ cover in areas with
564 high observed values, and overestimate cover in areas with low or zero measured herbaceous
565 C₄ cover. There are several possible explanations for this pattern. Analysis revealed most
566 TERN plots were dominated by either C₃ or C₄ herbaceous cover. Because mixed C₃-C₄
567 herbaceous environments were less common, they were invariably harder to predict. Lastly,
568 most climate data were centred on the year 1990, which may be less applicable for more
569 recent plots, leading to higher overall error rates. Most importantly, although we considered a
570 range of local factors in our C₄ cover models, models did not include other factors which may
571 also modify C₄ patterns but cannot currently be extrapolated at large scales, such as local
572 disturbance, soil salinity, and competition between native and alien species (Griffith et al.
573 2015; Sage et al. 1999).

574

575 A critical source of potential error in our final vegetation maps was the *% woody vegetation*
576 layer, generated using the Seasonal Persistent Green Cover product (Gill et al. 2017; Gill et
577 al. 2015). While the overall accuracy of the Seasonal Persistent Green Cover product is
578 impressive, Gill et al. (2017) noted that accuracy varied significantly between habitat types.
579 This was evident when comparing C₄ cover model accuracy between different major
580 vegetation groups. We found our C₄ estimates were least accurate in *Acacia*-dominated
581 habitats. These higher error rates are consistent with Gill et al. (2017), who found most areas
582 identified as *Acacia* forests, woodlands, and open woodlands were not mapped as forest.
583 Instead, they were incorrectly classed as having very low or no woody cover. Gill et al.

584 (2017) suggested several explanations for this issue; vegetation cover in *Acacia*-dominated
585 habitats can be sparse, which can make woody cover more difficult to detect. At thresholds of
586 <10% woody cover it was difficult to distinguish woody and non-woody vegetation (Gill et
587 al. 2017). Therefore, it can be more difficult to accurately assess woody cover, and
588 proportional C₃ vegetation cover, in sparse areas. Some *Acacia* also have narrow, needle-like
589 leaves which are harder to detect via satellite, whereas other *Acacia* species are known to
590 drop their leaves in very dry conditions, resulting in a low minimum green cover-fraction
591 over the course of the year. Finally, the understory is often visible through the sparse *Acacia*
592 canopy. When the understory greens-up in response to rainfall, this can give the appearance
593 of a highly variable time series in green cover for *Acacia* foliage, leading to its
594 misclassification as non-woody. Unsurprisingly, the difficulties associated with measuring
595 *Acacia* woody cover in Australia using remote sensing led to a high degree of variation C₃
596 and C₄ cover estimates in *Acacia*-dominated habitats.

597
598 C₃:C₄ estimates were also less accurate in chenopod shrublands. Accurately estimating C₄
599 cover in these environments may be more difficult because chenopod shrublands are often
600 sparsely vegetated (Gill et al. 2017). Our approach also assumed all shrub cover had a C₃
601 pathway. But as previously discussed, C₄ chenopods can be locally common in Australian
602 shrublands. As a result, our approach may underestimate C₄ cover in these habitats. However,
603 our model residuals indicate C₄ cover is more likely to be overestimated in chenopod
604 shrublands, which suggests our assumption that all shrubs are C₃ is not the main source of
605 error in these habitats. More likely, it is the difficulty associated with accurately assessing
606 woody cover in these sparse environments.

607

608 Other potential sources of error include the high degree of variation in $\delta^{13}\text{C}$ values between
609 different C_3 species and environmental conditions (Kohn 2010). For example, rainfall, soil
610 pH, and leaf nitrogen area are all significant drivers of variation in global C_3 $\delta^{13}\text{C}$ values
611 (Cornwell et al. 2018). Variation in $\delta^{13}\text{C}$ values within the canopy will also affect the overall
612 accuracy of $\delta^{13}\text{C}$ isoscapes (Cheesman et al. 2020), however it is difficult to effectively
613 quantify and model these different sources of variation across Australia at this time.
614 Unsurprisingly, areas with the greatest standard deviation in $\delta^{13}\text{C}$ values were areas
615 dominated by C_3 vegetation reflecting the greater variability in the carbon isotopic
616 composition among C_3 plants.

617 **Future Improvements**

618 The accuracy of the $\delta^{13}\text{C}$ isoscape hinges on three main components; (1) estimates of woody
619 and herbaceous cover, (2) the $\text{C}_3:\text{C}_4$ herbaceous cover model, and (3) the endmember values
620 in the $\delta^{13}\text{C}$ -leaf mixing model. Gill et al. (2017) outlines multiple ways to improve estimates
621 of woody cover. The proportional herbaceous C_4 cover ~ climate model could be improved as
622 TERN increases its plot network and environmental representation. For example, establishing
623 plots in Tasmania or increasing the number of plots with more equal $\text{C}_3:\text{C}_4$ ratios would
624 improve model outcomes by increasing the amount of data from cool climates and
625 transitional habitats. TERN has also begun to regularly revisit existing plots to monitor
626 change over time. Revisits could be used to calculate average C_4 cover over multiple years
627 and seasons, which would make the plot data a more appropriate validation tool for average
628 C_4 vegetation and isoscape projections. This would also enable the creation of more
629 seasonally specific isoscapes, rather than a static annual average. More specific information
630 on crop commodities, namely the location of maize and sorghum, would also improve the
631 accuracy of C_3 and C_4 vegetation layers.

632

633 The $\delta^{13}\text{C}$ endmembers were based on $\delta^{13}\text{C}$ values from Munroe et al. (2020b). These values
634 were measured from species collected at TERN plots, making them a useful metric with
635 which to calculate Australian vegetation $\delta^{13}\text{C}$ endmembers. However, the plants measured by
636 Munroe et al. (2020b) were not necessarily dominant or wide spread. Measuring the $\delta^{13}\text{C}$ of
637 the most common plants in TERN plots, and incorporating a wider range of herbaceous and
638 woody species, may help create endmembers that are better representations of dominant
639 Australian plant $\delta^{13}\text{C}$ values. Testing specimens that were collected under different
640 conditions (e.g. rainfall or soil pH) would enable expansion of the current mixing model to
641 account for different climate conditions when predicting $\delta^{13}\text{C}$ values, particularly in C_3
642 species (Cornwell et al. 2018).

643

644 **Applications**

645 The terrestrial carbon isoscape and C_3 and C_4 maps presented here have numerous valuable
646 applications. As demonstrated in this study, C_3 , C_4 and $\delta^{13}\text{C}$ maps can be used to quantify and
647 compare C_3 and C_4 distribution across different bioregions at a landscape scale. Such analysis
648 would not be possible without these data. Isoscapes are also enormously useful in the study of
649 food web dynamics and animal migration (Hobson et al. 2010; Vander Zanden et al. 2018;
650 Wunder 2010). These maps could also be used to calculate fractional productivity of different
651 photosynthetic pathways (Powell et al. 2012).

652

653 TERN's expansive plot network provides the opportunity to not only identify, but also
654 quantify discrepancies between predicted and observed C_4 and C_3 cover. Indeed, our work
655 has already demonstrated the importance of some edaphic factors in controlling C_4
656 distribution. As more data becomes available, further comparisons across a wider range of
657 factors will be possible. Similarly, differences in predicted $\delta^{13}\text{C}$ values and local vegetation

658 can be used to examine the influence of local factors, such as water stress or drought, on $\delta^{13}\text{C}$
659 values (Ehleringer 1993; Mårtensson et al. 2017; Tieszen 1991).

660

661 Climate change is anticipated to drastically shift the competitive advantage of C_3 and C_4
662 plants in Australia and globally, leading to substantial changes in species distribution (Corlett
663 and Westcott 2013; Hasegawa et al. 2018). This will likely drive significant bottom-up
664 changes to the structure and diversity of faunal communities (Haddad et al. 2009; Haveles et
665 al. 2019; Warne et al. 2010). Using our underlying climate models, C_3 and C_4 abundance can
666 be extrapolated under future conditions and areas that are most vulnerable to extreme changes
667 in C_3 and C_4 cover can be identified. Our models identified maximum temperature and
668 seasonal water availability as the two most significant climate factors driving C_3 and C_4
669 herbaceous cover in Australia. Based on these findings, we would expect to see considerable
670 expansion of C_4 suitable climate-zones in southern Australia. Historically, southern Australia
671 has a Mediterranean climate, with dry summers and higher winter rainfall. However, the
672 climate in southern Australia is expected to become increasingly dry, with hotter
673 temperatures and more frequent heatwaves (Keywood et al. 2017; Suppiah et al. 2006),
674 conditions that are better suited to C_4 species. These models will also improve our ability to
675 quantify potentially improved conditions for invasive species, such as the invasive C_4 buffel
676 grass, *Cenchrus ciliaris* L. (de Albuquerque et al. 2019; Lawson et al. 2004). Forecasting
677 native C_3 and C_4 abundance can also enable proactive environmental management in
678 Australia's changing climate, such as identifying suitable locations for future C_4 and C_3 crops
679 (Cullen et al. 2009) or important refuge areas for native plant communities (Graham et al.
680 2019; Selwood and Zimmer 2020).

681

682 **Conclusion**

683 We have applied a novel combination of detailed ground survey, climate, and remote sensing
684 data to create and evaluate the first Australian vegetation $\delta^{13}\text{C}$ isoscape. These results have a
685 wide range of applications, including the study of animal migration, food web patterns,
686 spatial and temporal variation in plant productivity and habitat structure, carbon exchange,
687 and the impact of water stress on plant communities. Our continued ability to test and
688 validate these models as new TERN plots and isotope data become available provides a
689 unique opportunity to develop future improvements. The C_3 , C_4 and isoscape maps presented
690 here were created to support the study of Australian ecosystems and have enormous value to
691 broader ecological research. It is our intention to curate and update these outputs where
692 possible as new TERN plots and isotope data become available.

693

DRAFT

694

695 **References**

696 ABARES (2016) The Australian Land Use and Management Classification Version 8.

697 Australian Bureau of Agricultural and Resource Economics and Sciences, Canberra

698 ABS (2016) Agricultural Commodities, Australia, 2015-16. In: ABS (ed). ABS, Canberra

699 Akhani H, Trimborn P, Ziegler H (1997) Photosynthetic pathways in Chenopodiaceae from

700 Africa, Asia and Europe with their ecological, phytogeographical and taxonomical

701 importance. *Plant Syst Evol* 206:187-221

702 Atkins R (2021) Soil carbon isotopic proxies for determining the photosynthetic pathway of

703 floral communities: A method inter-comparison. Doctoral dissertation, University of

704 Adelaide

705 Bataille CP, von Holstein ICC, Laffoon JE, Willmes M, Liu X-M, Davies GR (2018) A

706 bioavailable strontium isoscape for Western Europe: A machine learning approach.

707 *PLOS ONE* 13:e0197386

708 Ben-David M, Flaherty EA (2012) Stable isotopes in mammalian research: a beginner's

709 guide. *J Mammal* 93:312-328

710 Bromham L, Saslis-Lagoudakis CH, Bennett TH, Flowers TJ (2013) Soil alkalinity and salt

711 tolerance: adapting to multiple stresses. *Biol Lett* 9:20130642

712 Cernusak LA (2020) Gas exchange and water-use efficiency in plant canopies. *Plant Biol*

713 22:52-67

714 Cheesman AW, Duff H, Hill K, Cernusak LA, McInerney FA (2020) Isotopic and

715 morphologic proxies for reconstructing light environment and leaf function of fossil

716 leaves: a modern calibration in the Daintree Rainforest, Australia. *Am J Bot*

717 107:1165-1176

718 Cole PG, Weltzin JF (2005) Light limitation creates patchy distribution of an invasive grass
719 in eastern deciduous forests. *Biol Invasions* 7:477-488

720 Collatz GJ, Berry JA, Clark JS (1998) Effects of climate and atmospheric CO₂ partial
721 pressure on the global distribution of C₄ grasses: present, past, and future. *Oecologia*
722 114:441-454

723 Corlett RT, Westcott DA (2013) Will plant movements keep up with climate change? *Trends*
724 *Ecol Evol* 28:482-488

725 Cornwell WK, Wright IJ, Turner J et al (2018) Climate and soils together regulate
726 photosynthetic carbon isotope discrimination within C₃ plants worldwide. *Glob Ecol*
727 *Biogeogr* 27:1056-1067

728 Cullen BR, Johnson IR, Eckard RJ et al (2009) Climate change effects on pasture systems in
729 south-eastern Australia. *Crop Pasture Sci* 60:933-942

730 de Albuquerque FS, Macías-Rodríguez MÁ, Búrquez A, Astudillo-Scalia Y (2019) Climate
731 change and the potential expansion of buffelgrass (*Cenchrus ciliaris* L., Poaceae) in
732 biotic communities of Southwest United States and northern Mexico. *Biol Invasions*
733 21:3335-3347

734 Department of Agriculture, Water and the Environment (2020), Interim Biogeographic
735 Regionalisation for Australia (Regions - States and Territories) v. 7 (IBRA)

736 Dormann CF, Bagnara M, Boch S et al (2020) Plant species richness increases with light
737 availability, but not variability, in temperate forests understorey. *BMC Ecology* 20:43

738 Douma JC, Weedon JT (2019) Analysing continuous proportions in ecology and evolution: A
739 practical introduction to beta and Dirichlet regression. *Method Ecol Evo* 10:1412-
740 1430

741 Ehleringer JR (1978) Implications of quantum yield differences on the distributions of C₃ and
742 C₄ grasses. *Oecologia* 31:255-267

743 Ehleringer JR (1993) 11 - Carbon and Water Relations in Desert Plants: An Isotopic
744 Perspective. In: Ehleringer J. R., Hall A. E., Farquhar G. D. (eds), Stable Isotopes and
745 Plant Carbon-water Relations. Academic Press, San Diego, pp. 155-172

746 Firmin SM (2016) The spatial distribution of terrestrial stable carbon isotopes in North
747 America, and the impacts of spatial and temporal resolution on static ecological
748 models. University of Denver

749 Flockhart DTT, Brower LP, Ramirez MI et al (2017) Regional climate on the breeding
750 grounds predicts variation in the natal origin of monarch butterflies overwintering in
751 Mexico over 38 years. *Glob Change Biol* 23:2565-2576

752 Frank DC, Poulter B, Saurer M et al (2015) Water-use efficiency and transpiration across
753 European forests during the Anthropocene. *Nat Clim Change* 5:579-583

754 Gallant J, Austin J, Williams K et al (2018) 9s soil and landform for continental Australia
755 analysis of biodiversity pattern: aggregated from 3s data. v1. CSIRO,

756 Gill T, Johansen K, Phinn S, Trevithick R, Scarth P, Armston J (2017) A method for mapping
757 Australian woody vegetation cover by linking continental-scale field data and long-
758 term Landsat time series. *Int J Remote Sens* 38:679-705

759 Gill T, Johansen K, Scarth P, Armston J, Trevithick R, Flood N (2015) Persistent Green
760 Vegetation Fraction. In: Held A., Phinn S., Soto-Berelov M., Jones S. (eds),
761 AusCover Good Practice Guidelines: A technical handbook supporting calibration
762 and validation activities of remotely sensed data products. . TERN AusCover, pp.
763 139-160

764 Graham V, Baumgartner JB, Beaumont LJ, Esperón-Rodríguez M, Grech A (2019)
765 Prioritizing the protection of climate refugia: designing a climate-ready protected area
766 network. *J Environ Plan Manag* 62:2588-2606

767 Griffith DM, Anderson TM, Osborne CP, Strömberg CA, Forrestel EJ, Still CJ (2015)
768 Biogeographically distinct controls on C₃ and C₄ grass distributions: merging
769 community and physiological ecology. *Glob Ecol Biogeogr* 24:304-313

770 Griffith DM, Rebecca L Powell, Firmin S, Cotton J, Still CJ (2019) grassmapr, an R package
771 to predict C₃/C₄ grass distributions and model terrestrial $\delta^{13}\text{C}$ isoscapes. R Package
772 version 1 edn.,

773 Guélat J, Kéry M (2018) Effects of spatial autocorrelation and imperfect detection on species
774 distribution models. *Method Ecol Evo* 9:1614-1625

775 Guerin GR, Saleeba T, Munroe S, Blanco-Martin B, Martín-Forés I, Tokmakoff A (2020)
776 ausplotsR: TERN AusPlots analysis package. R Package version 1.2 edn.,

777 Haddad NM, Crutsinger GM, Gross K, Haarstad J, Knops JMH, Tilman D (2009) Plant
778 species loss decreases arthropod diversity and shifts trophic structure. *Ecol Lett*
779 12:1029-1039

780 Hasegawa S, Piñeiro J, Ochoa-Hueso R et al (2018) Elevated CO₂ concentrations reduce C₄
781 cover and decrease diversity of understorey plant community in a Eucalyptus
782 woodland. *J Ecol* 106:1483-1494

783 Hattersley P (1983) The distribution of C₃ and C₄ grasses in Australia in relation to climate.
784 *Oecologia* 57:113-128

785 Haveles AW, Fox DL, Fox-Dobbs K (2019) Carbon isoscapes of rodent diets in the Great
786 Plains USA deviate from regional gradients in C₄ grass abundance due to a preference
787 for C₃ plant resources. *Palaeogeogr Palaeoclimatol Palaeoecol* 527:53-66

788 Hobson KA, Barnett-Johnson R, Cerling T (2010) Using isoscapes to track animal migration.
789 In: West J., Bowen G., Dawson T., Tu K. (eds), *Isoscapes*. Springer, Dordrecht, pp.
790 273-298

791 Hobson KA, Kardynal KJ (2015) An isotope ($\delta^{34}\text{S}$) filter and geocator results constrain a
792 dual feather isoscape ($\delta^2\text{H}$, $\delta^{13}\text{C}$) to identify the wintering grounds of North American
793 Barn Swallows. *The Auk* 133:86-98

794 Hobson KA, Wassenaar LI (2018) Tracking animal migration with stable isotopes, 2nd
795 Edition. Academic Press, London

796 James JJ, Tiller RL, Richards JH (2005) Multiple resources limit plant growth and function in
797 a saline-alkaline desert community. *J Ecol* 93:113-126

798 Kellogg EA (2001) Evolutionary history of the grasses. *Plant Physiol* 125:1198-1205

799 Kelly JF (2000) Stable isotopes of carbon and nitrogen in the study of avian and mammalian
800 trophic ecology. *Can J Zool* 78:1-27

801 Keywood M, Hibberd M, Emmerson K (2017) Australia state of the environment 2016:
802 atmosphere, independent report to the Australian Government Minister for the
803 Environment and Energy, Australian Government Department of the Environment
804 and Energy, Canberra. Canberra,

805 Kohn MJ (2010) Carbon isotope compositions of terrestrial C_3 plants as indicators of
806 (paleo)ecology and (paleo)climate. *PNAS* 107:19691-19695

807 Krull EG, Bray, SS (2005) Assessment of vegetation change and landscape variability by
808 using stable carbon isotopes of soil organic matter. *Aus J Bot*, 53:651-661
809 doi:10.1071/bt04124

810 Lawson B, Bryant M, Franks A (2004) Assessing the potential distribution of buffel grass
811 (*Cenchrus ciliaris* L.) in Australia using a climate-soil model. *Plant Prot Q* 19:155-
812 163

813 López-Calderón C, Hobson KA, Marzal A et al (2017) Wintering areas predict age-related
814 breeding phenology in a migratory passerine bird. *J Avian Biol* 48:631-639

815 Mårtensson L-M, Carlsson G, Prade T, Kørup K, Lærke PE, Jensen ES (2017) Water use
816 efficiency and shoot biomass production under water limitation is negatively
817 correlated to the discrimination against ^{13}C in the C_3 grasses *Dactylis glomerata*,
818 *Festuca arundinacea* and *Phalaris arundinacea*. 113:1-5

819 Matthews JL, Diawara N, Waller LA (2019) Quantifying spatio-temporal characteristics via
820 Moran's statistics. In: Diawara N. (ed), Modern statistical methods for spatial and
821 multivariate data. Springer International Publishing, Cham, pp. 163-177

822 Mets KD, Armenteras D, Dávalos LM (2017) Spatial autocorrelation reduces model precision
823 and predictive power in deforestation analyses. *Ecosphere* 8:e01824

824 Munroe S, Guerin G, Saleeba T et al (2020a) *ausplotsR*: An R package for rapid extraction
825 and analysis of vegetation and soil data collected by Australia's Terrestrial Ecosystem
826 Research Network. *EcoEvoRxiv*.

827 Munroe S, McInerney F, Andrae J et al (2020b) The photosynthetic pathways of plant species
828 surveyed in Australia's national terrestrial monitoring network.

829 Munroe SEM, McInerney FA, Guerin GR et al (2022) Plant families exhibit unique trends in
830 C_4 richness and abundance. *EcoEvoRxiv* doi:10.32942/osf.io/vxu6s.

831 Murphy BP, Bowman DM (2007) Seasonal water availability predicts the relative abundance
832 of C_3 and C_4 grasses in Australia. *Glob Ecol Biogeogr* 16:160-169

833 Nippert JB, Knapp AK (2007) Soil water partitioning contributes to species coexistence in
834 tallgrass prairie. *Oikos* 116:1017-1029

835 O'Leary MH (1988) Carbon isotopes in photosynthesis. *Bioscience* 38:328-336

836 O'Neill AL (1996) Satellite-derived vegetation indices applied to semi-arid shrublands in
837 Australia. *Aust Geogr* 27:185-199

838 Pate JS, Unkovich MJ, Erskine PD, Stewart GR (1998) Australian mulga ecosystems –¹³C
839 and ¹⁵N natural abundances of biota components and their ecophysiological
840 significance. *Plant Cell Environ* 21:1231-1242

841 Pau S, Edwards EJ, Still CJ (2013) Improving our understanding of environmental controls
842 on the distribution of C₃ and C₄ grasses. *Glob Change Biol* 19:184-196

843 Powell RL, Yoo E-H, Still CJ (2012) Vegetation and soil carbon-13 isoscapes for South
844 America: integrating remote sensing and ecosystem isotope measurements. *Ecosphere*
845 3:1-25

846 Prober SM, Thiele KR, Lunt ID (2007) Fire frequency regulates tussock grass composition,
847 structure and resilience in endangered temperate woodlands. *Austral Ecol* 32:808-824

848 Sage RF (2004) The evolution of C₄ photosynthesis. *New Phytol* 161:341-370

849 Sage RF (2016) A portrait of the C₄ photosynthetic family on the 50th anniversary of its
850 discovery: species number, evolutionary lineages, and hall of fame. *J Exp Bot* 68:11-
851 28

852 Sage RF, Sage TL, Kocacinar F (2012) Photorespiration and the evolution of C₄
853 photosynthesis. *Ann Rev Plant Biol* 63:19-47

854 Sage RF, Wedin DA, Li M (1999) The biogeography of C₄ photosynthesis: patterns and
855 controlling factors. In: Sage R. F. and Monson R. K. (eds), *C₄ plant biology*. Academic
856 Press, Sydney, pp. 313-373

857 Salsis-Lagoudakis CH, Hua X, Bui E, Moray C, Bromham L (2014) Predicting species'
858 tolerance to salinity and alkalinity using distribution data and geochemical modelling:
859 a case study using Australian grasses. *Ann Bot* 115:343-351

860 Selwood KE, Zimmer HC (2020) Refuges for biodiversity conservation: a review of the
861 evidence. *Biol Conserv* 245:108502

862 Sparrow AD, Friedel MH, Smith DMS (1997) A landscape-scale model of shrub and herbage
863 dynamics in Central Australia, validated by satellite data. *Ecol Model* 97:197-216

864 Sparrow BD, Foulkes JN, Wardle GM et al (2020) A vegetation and soil survey method for
865 surveillance monitoring of rangeland environments. *Front Ecol Evol* 8

866 Still C, Rastogi B (2017) What drives carbon isotope fractionation by the terrestrial
867 biosphere? *J Geophys Res Biogeosci* 122:3108-3110

868 Still CJ, Berry JA, Collatz GJ, DeFries RS (2003) Global distribution of C₃ and C₄
869 vegetation: carbon cycle implications. *Global Biogeochem Cy* 17:1006

870 Still CJ, Powell RL (2010) Continental-scale distributions of vegetation stable carbon isotope
871 ratios. *Isoscapes*. Springer, pp. 179-193

872 Suppiah R, Preston B, Whetton P et al (2006) Climate change under enhanced greenhouse
873 conditions in South Australia.

874 Tieszen LL (1991) Natural variations in the carbon isotope values of plants: Implications for
875 archaeology, ecology, and paleoecology. *18:227-248*

876 Tieszen LL, Boutton TW, Tesdahl KG, Slade NA (1983) Fractionation and turnover of stable
877 carbon isotopes in animal tissues: Implications for $\delta^{13}\text{C}$ analysis of diet. *Oecologia*
878 *57:32-37*

879 Trevithick R, Scarth P, Tindall D, Denham R, Flood N (2014) Cover under trees: RP64G
880 Synthesis Report. Department of Science, Information Technology, Innovation and
881 the Arts, Brisbane,

882 Vander Zanden HB, Nelson DM, Wunder MB, Conkling TJ, Katzner T (2018) Application of
883 isoscapes to determine geographic origin of terrestrial wildlife for conservation and
884 management. *Biol Conserv* 228:268-280

885 von Fischer JC, Tieszen LL, Schimel DS (2008) Climate controls on C₃ vs. C₄ productivity in
886 North American grasslands from carbon isotope composition of soil organic matter.
887 Glob Change Biol 14:1141-1155

888 Wang K, Zhong S, Sun W (2020) Clipping defoliation and nitrogen addition shift
889 competition between a C₃ grass (*Leymus chinensis*) and a C₄ grass (*Hemarthria*
890 *altissima*). Plant Biol 22:221-232

891 Warne RW, Pershall AD, Wolf BO (2010) Linking precipitation and C₃-C₄ plant production
892 to resource dynamics in higher-trophic-level consumers. Ecology 91:1628-1638

893 West JB, Bowen GJ, Dawson TE, Tu KP (2009) Isoscapes: understanding movement,
894 pattern, and process on Earth through isotope mapping. Springer, Dordrecht

895 White A, Sparrow B, Leitch E et al (2012) AUSPLOTS rangelands survey protocols manual.
896 The University of Adelaide Press, Adelaide

897 Williams K, Stein J, Storey R et al (2010) 0.01 degree stack of climate layers for continental
898 analysis of biodiversity pattern. version 1.0 edn. CSIRO

899 Winslow JC, Hunt Jr ER, Piper SC (2003) The influence of seasonal water availability on
900 global C₃ versus C₄ grassland biomass and its implications for climate change
901 research. Ecol Model 163:153-173

902 Wood S (2006) GAMMs with R. Chapman & Hall/CRC, New York, NY

903 Wood S (2021) Mixed GAM computation vehicle with automatic smoothness estimation. R
904 Package version 18-35 edn.

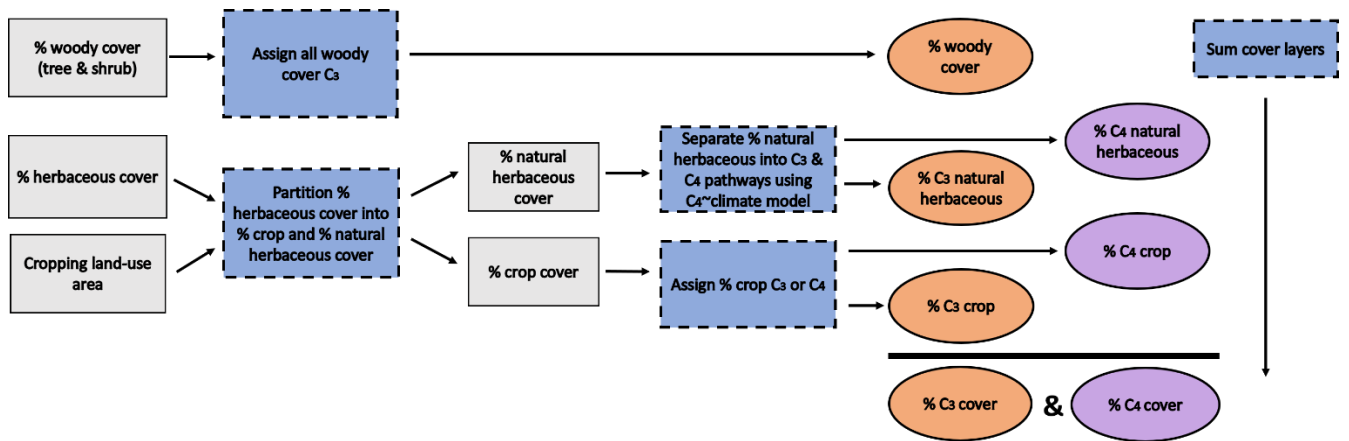
905 Wood SN (2017) Generalized additive models: an introduction with R. CRC press, Boca
906 Raton

907 Wunder MB (2010) Using isoscapes to model probability surfaces for determining
908 geographic origins. In: West J. B., Bowen G. J., Dawson T. E., Tu K. P. (eds),
909 Isoscapes. Springer, Dordrecht, pp. 251-270

910 Xie Q, Huete A, Hall CC, Medlyn BE, Power SA, Davies JM, et al. Satellite-observed shifts
911 in C_3/C_4 abundance in Australian grasslands are associated with rainfall patterns.
912 Remote Sens Environ. 273:112983. doi: <https://doi.org/10.1016/j.rse.2022.112983>.
913 Zuur AF, Ieno EN, Walker NJ, Saveliev AA, Smith GM (2009) GLMM and GAMM. Mixed
914 effects models and extensions in ecology with R. Springer New York, New York,
915 NY, pp. 323-341

DRAFT

916 **Figures**



917

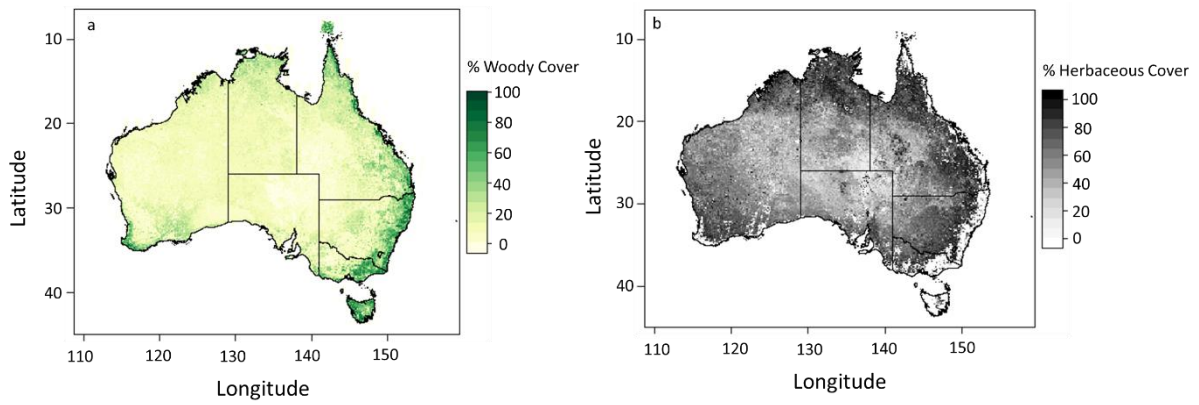
918

919 **Fig 1.** Conceptual diagram of the procedures used to create each C₃ and C₄ vegetation cover
 920 layer. Grey boxes specify generic vegetation layers, blue boxes specify steps in the
 921 methodology, orange ovals are the resulting C₃ vegetation cover layers, purple ovals are C₄
 922 vegetation cover layers. All C₃ and C₄ layers were summed to create a total ‘% C₄ cover’ and
 923 ‘% C₃ cover’ layer

924

DRAFT

925



926

927

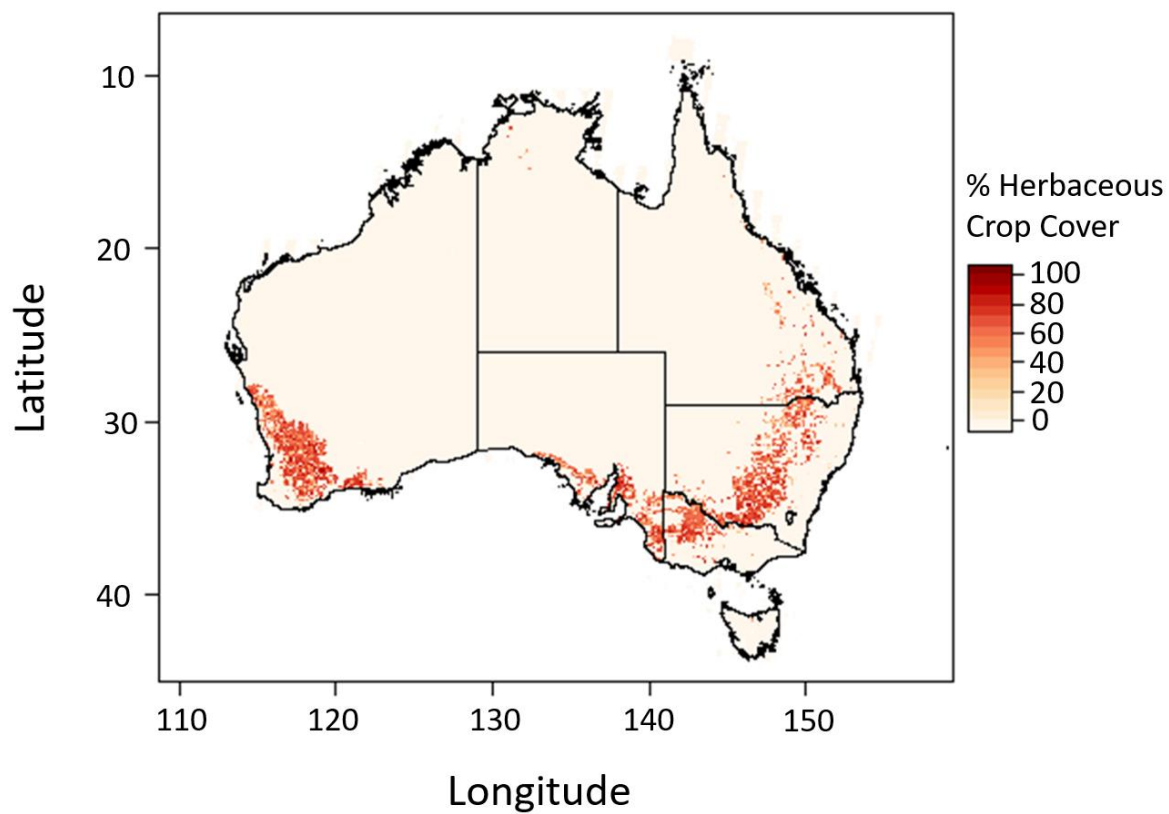
928

929

Fig. 2. Mean Australian (a) % woody cover (tree and shrub) and (b) % herbaceous cover in 2015

DRAFT

930



931

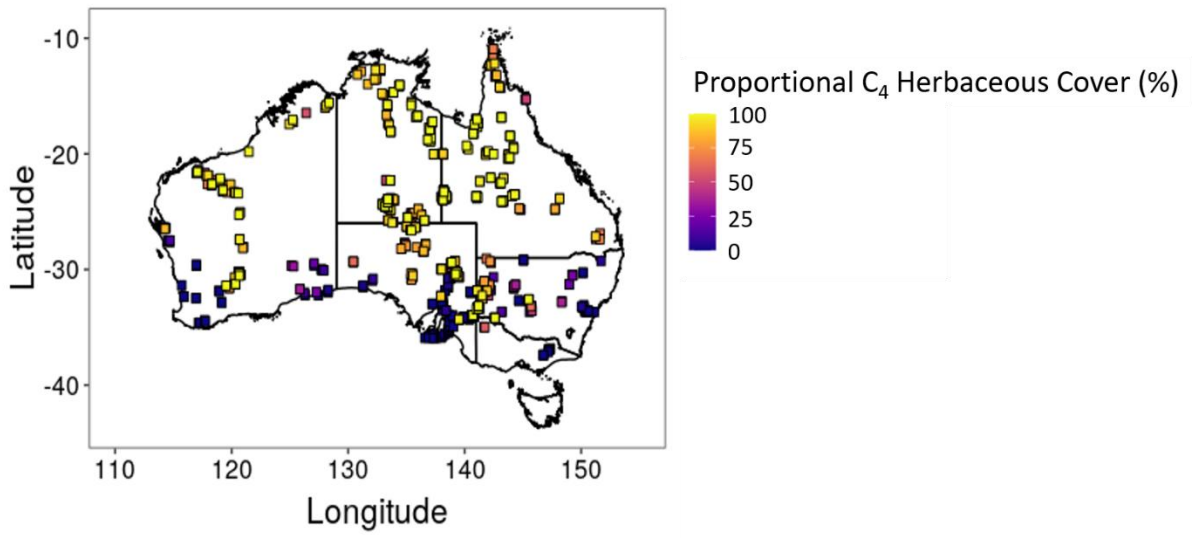
932

Fig. 3. Australian % herbaceous crop cover as of December 2018

933

DRAFT

934

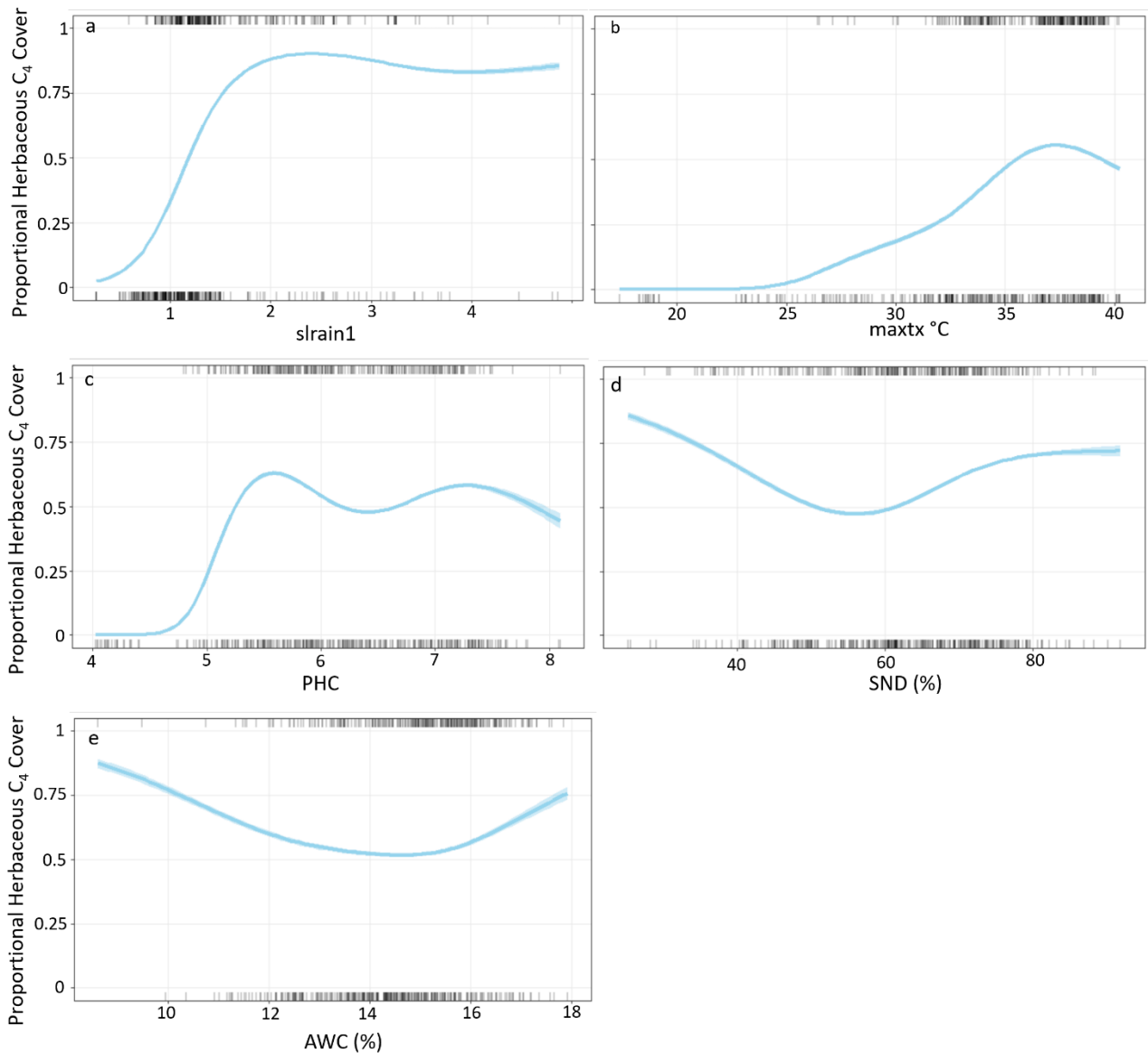


935

936 **Fig. 4.** Proportional (%) herbaceous C₄ cover (relative to herbaceous C₃ and C₄ cover) at
937 TERN plots

938

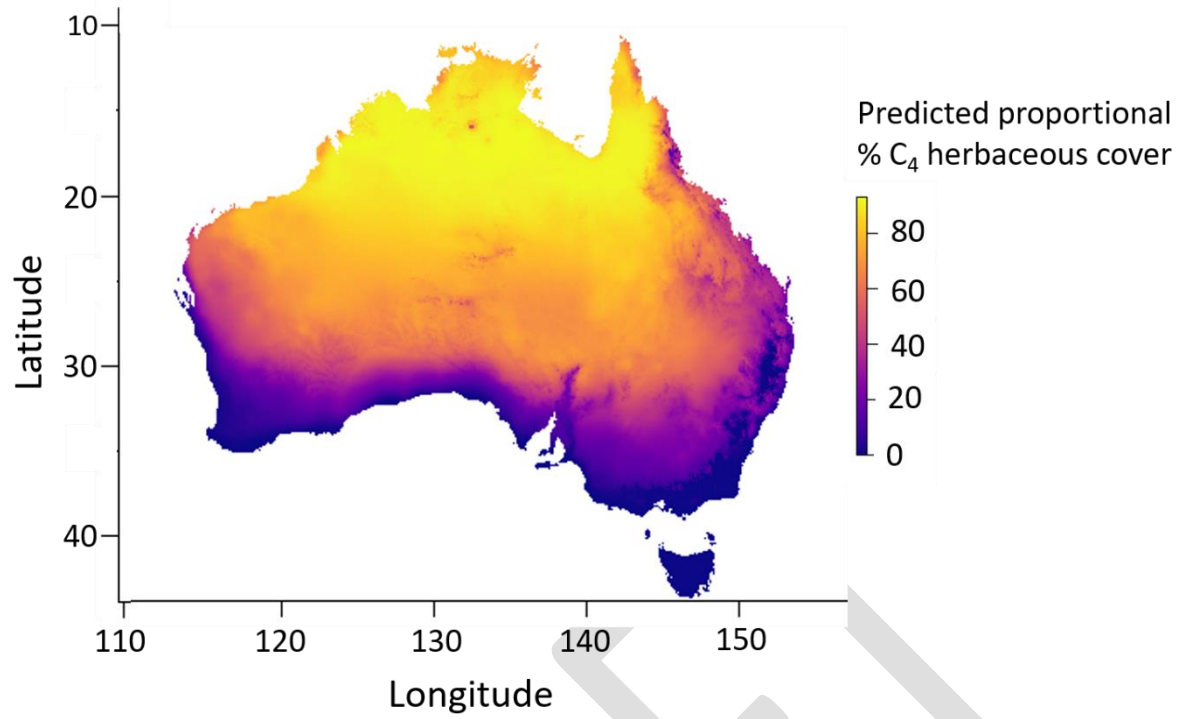
DRAFT



939

940 **Fig. 5.** Predicted proportional herbaceous C₄ Cover (relative to herbaceous C₃ and C₄
 941 herbaceous cover) against the explanatory variables (a) slrain1 (The ratio (log) of summer
 942 (Dec-Jan-Feb) to winter (Jun-Jul-Aug) rainfall totals) (b) maxtx (Maximum temperature
 943 hottest month (°C) , (c) PHC (Soil pH-CaCl₂) (d) AWC (soil available water capacity %),
 944 and (e) SND (soil sand content %) derived from a GAM model constructed using TERN
 945 vegetation survey plot data. Blue lines are predicted outcomes of the model. Rugs were
 946 drawn to indicate observations with positive residuals (top of the plot) or negative residuals
 947 (bottom of the plot). Independent variables not depicted on the x-axis are held constant at
 948 their median value

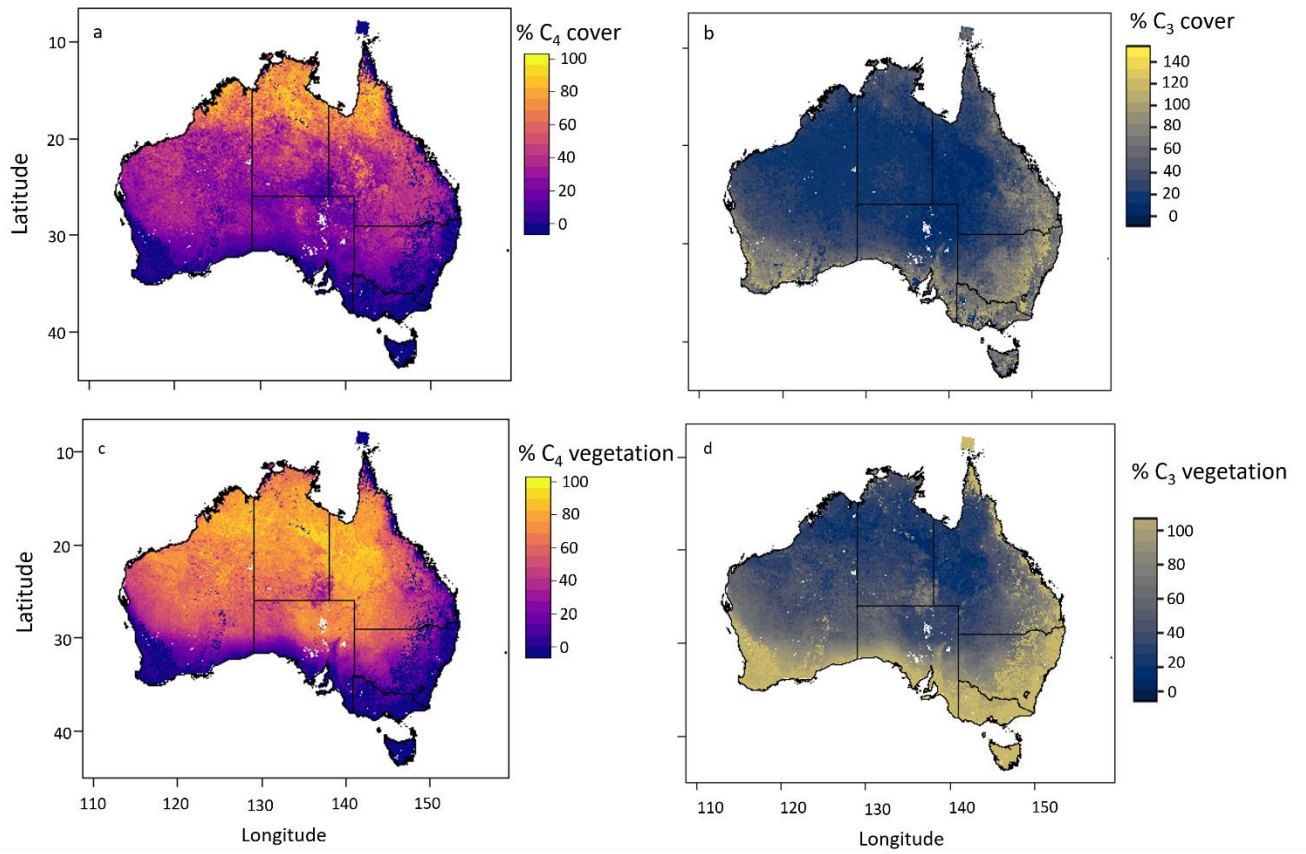
949



950
951
952
953

Fig 6. Predicted proportional (%) herbaceous C₄ cover (relative to herbaceous C₃ and C₄ herbaceous cover) extrapolated across Australia

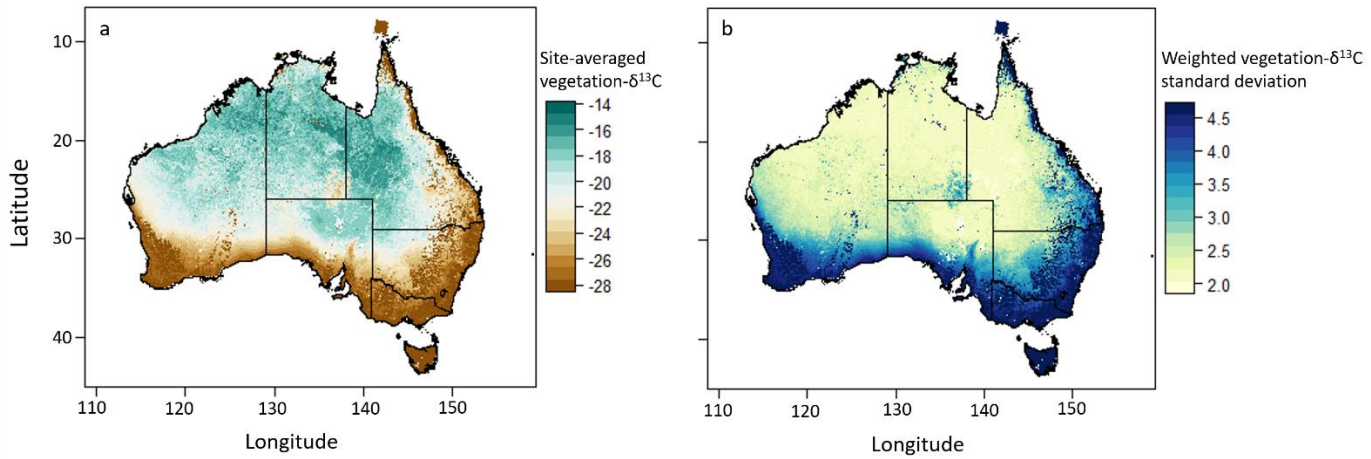
DRAFT



954

955 **Fig. 7.** % (a) C₄ and (b) C₃ cover, and proportional (c) C₄ and (d) C₃ vegetation cover
 956 (proportional to total vegetation) in 2015

957



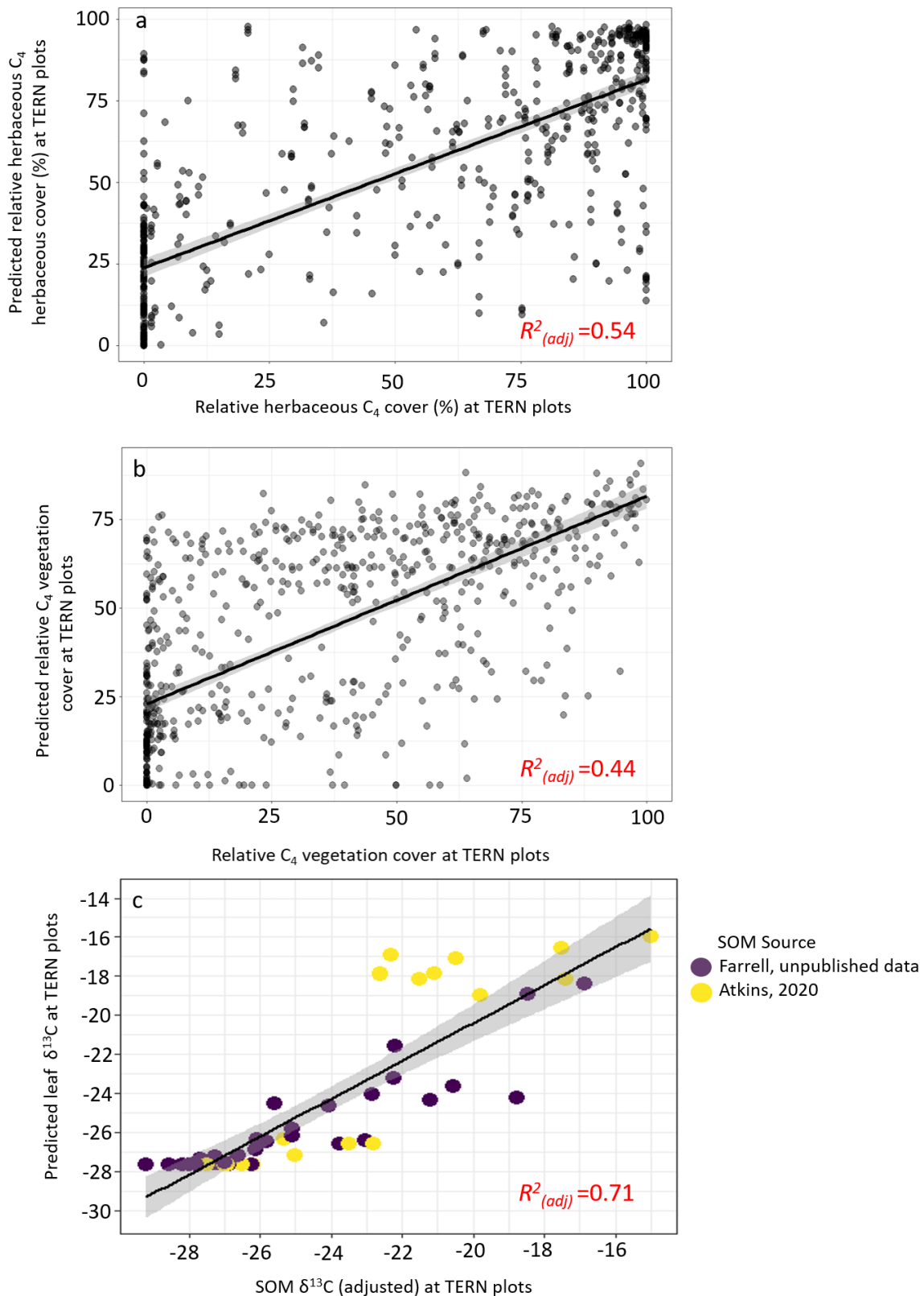
958

959 **Fig. 8.** a) Vegetation $\delta^{13}\text{C}$ isoscape of Australia corresponding to the year 2015 and b)
960 weighted mean standard deviation of site-averaged $\delta^{13}\text{C}$ values

961

962

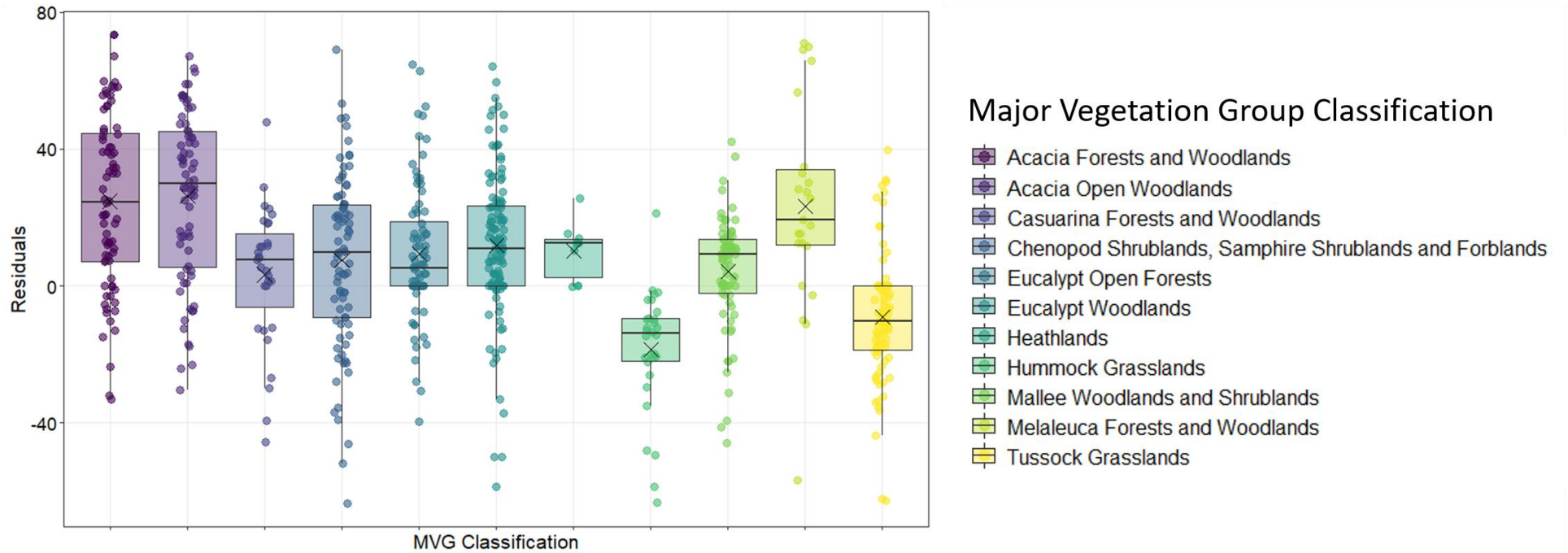
DRAFT



963

964 **Fig 9.** (a) Scatter plot of observed versus predicted relative % herbaceous C₄ Cover (relative
 965 to herbaceous C₃ cover) at TERN plots from 10-fold cross validation testing dataset, (b)
 966 predicted and observed relative C₄ vegetation cover (including woody cover) at all TERN
 967 plots, c) predicted leaf-δ¹³C and measured Soil Organic Matter δ¹³C at select TERN plots

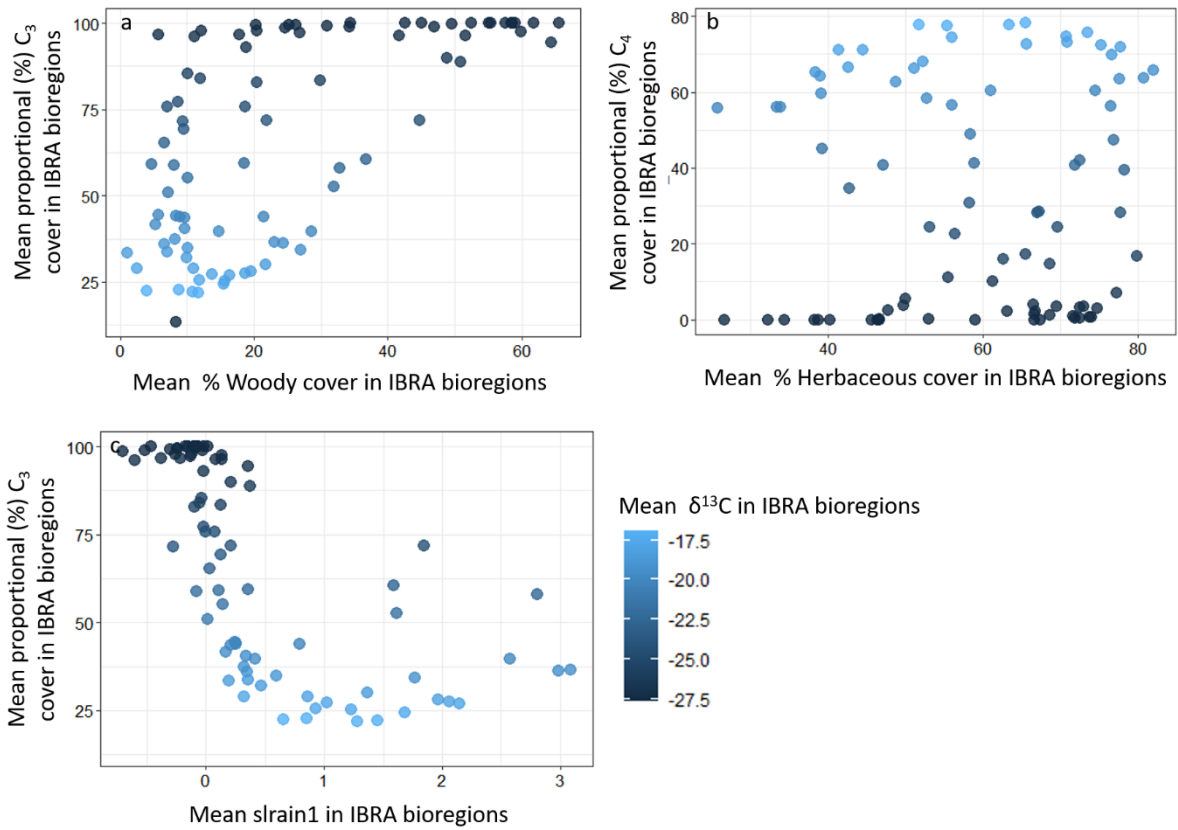
968



969

970

971 **Fig. 10** Residuals of predicted and observed % C₄ vegetation cover (relative to total cover and including woody cover) at all TERN plots in
972 major vegetation group (MVG) classifications. The box defines the second and third quartiles (likely range of variation), the vertical lines are the
973 upper and lower quartiles. The black bands are the median residual values, the black X is the mean residual value for each classification.



974

975 **Fig. 11.** (a) Scatterplot of predicted mean proportional C₃ Cover versus mean % woody cover
 976 (tree and shrub) across 86 different continental Australian bioregions, as described by the
 977 interim Biogeographic Regionalisation for Australia version 7 (IBRA 7.0; Department of
 978 Agriculture, Water and the Environment, 2020); (b) Scatterplot of predicted mean
 979 proportional C₄ Cover versus mean % herbaceous cover in different IBRA 7.0 ; (c)
 980 Scatterplot of predicted mean proportional C₃ cover versus mean slrain1 (The ratio (log) of
 981 summer (Dec-Jan-Feb) to winter (Jun-Jul-Aug) rainfall totals) across IBRA 7.0

982

983

984

985 **Supplemental Matieral Captions**

986 1. Supplemental Methods

987 2. Supplemental Results

988 3. Supplemental Results, IBRA Analysis

989

990

DRAFT